

Seakeeping control of HYSUCATs

by

Giovanni Sergio Milandri

*Thesis presented at the University of Stellenbosch in
partial fulfilment of the requirements for the degree
of*

Master of Science in Mechanical Engineering



Department of Mechanical Engineering
University of Stellenbosch
Private Bag X1, 7602 Matieland, South Africa

Study leaders:

Prof Johannes L. van Niekerk Dr Gunther Migeotte
Dept of Mechanical Engineering Unistel Technologies (Pty) Ltd
University of Stellenbosch

March 2006

Declaration

I, the undersigned, hereby declare that the work contained in this thesis is my own original work and that I have not previously in its entirety or in part submitted it at any university for a degree.

Signature:

G.S. Milandri

Date:



Abstract

Seakeeping control of HYSUCATs

G.S. Milandri

Department of Mechanical Engineering

University of Stellenbosch

Private Bag XI, 7602 Matieland, South Africa

Thesis: MScEng (Mech)

March 2006

This thesis investigates practical methods of modelling and control of the vertical motions of a hydrofoil assisted catamaran, the HYSUCAT. The aim of the control application is to reduce the motions, and consequently the motion sickness of the passengers.

First, a potential flow commercial program, POWERSEA, was used to model the system. This uses 2-D strip methods to model the planing hull-form of the vessel, and the Peter du Cane hydrofoil theory for modelling of the foils. These simulations are compared to experimental towing tank results, with fair agreement at lower speeds, but limited applicability at high speeds. Thus for the control design the agreement was insufficient.

As an alternative, a simple coupled 2 degree-of-freedom spring - mass - damper model is proposed, for which the equations of motion are derived. This has 9 unknown parameters; three of these are measured directly, two are modelled, and the remaining four were identified using an experimental parameter estimation technique. Representative parameter values were calculated from multiple experiments for application in the control design.

The design of a control system was based on the above model. First, an output-weighted Linear Quadratic Regulator (LQR) was designed to obtain the full state feedback gains. A non-linear 'bang-bang' control design was then implemented to try and speed up the response of the system. These control strategies, as well as no control, were applied in the towing tank in regular waves, with good results at low and medium frequencies. At the design point, 32% and 65% reductions in rms motions were achieved for pitch and heave, respectively. At high frequencies, though, not much improvement was achieved due to the bandwidth limitation of the control system. The LQR results were better overall (reduced motions) across the frequency range than the bang-bang controller, as well as having a lower added resistance in waves.

The control design of the output-weighted LQR was then revised to be based on alternative outputs, as a possible improvement. However, a further two controller designs did not yield any noticeable improvement and were not developed further.



Uittreksel

Die beheer van die seevaardigheid van 'n HYSUCAT

("Seakeeping Control of HYSUCATs")

G.S. Milandri

Departement Meganiese Ingenieurswese

Universiteit van Stellenbosch

Privaatsak X1, 7602 Matieland, Suid Afrika

Tesis: MScIng (Meg)

Maart 2006

Hierdie tesis handel oor die modellering en beheer van die 'vertikale vlak' bewegings van 'n waterblad gesteunde tweerompskuit, die HYSUCAT. Die doel van die beheerstoepassing is om die bewegings, en dus die rysiekte, van die passasiers te verminder.

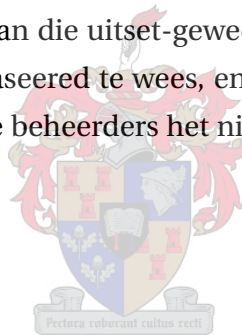
'n Potensiaal-vloei komersiële program, POWERSEA, was gebruik om die stelsel te modelleer. 'n 2-D 'skyfie metode' was toegepas om die skerende romp van die boot te simuleer, en Peter du Cane waterblad teorie was vir die waterblaaï simulasie gebruik. Die rekenaar simulasies word met eksperimentele sleeptenk resultate vergelyk en goeie ooreenstemming is by lae spoede verkry, maar is meer beperk by hoë spoede. Vir die beheerstoepassing was die resultate nie voldoende nie.

'n Alternatief was ondersoek deur die boot as 'n eenvoudige twee-vryheidsgraad veer-massa-demper model voor te stel. Die bewegingsvergelykings is afgelei en het nege onbekendes; drie van hulle word direk gemeet, twee word gemodelleer, en die oorblywende vier was geïdentifiseer met 'n eksperimen-

tele parameter skattings tegniek. Verteenwoordigende waardes word van eksperimente bereken om in die beheer ontwerp te gebruik.

Die ontwerp van 'n beheerstelsel was gebaseer op die laasgenoemde model. Eerstens, is 'n uitset-geweegde Lineëre Kwadratise Regulator (LKR) ontwerp om die terugvoer konstantes te bereken. 'n Nie-lineëre 'bang-bang' beheerder was toe ontwerp om die stelsel vinniger te maak. Hierdie beheerders, asook die geval sonder beheer, was toegepas in die sleeptenk in reëlmatige golwe, met goeie resultate by lae en natuurlike frekwensies. By die ontwerpspunt, was verminderinge van 32% vir die ζ -rigting en 65% vir die θ -rigting bereik. By hoë frekwensies, was min verbetering volgebring weens die tydsvertraging in die stelsel. Die LKR beheerder het in die algemeen kleiner bewegings oor die hele frekwensie gebied as die 'bang-bang' beheerder, asook laer bygevoegde weerstand.

Die beheerder ontwerp van die uitset-geweegde LKR was toe hersien om op alternatiewe uitsette gebaseer te wees, en om dalk die prestasie te verbeter. Maar, die verdere twee beheerders het nie beter gevaar nie, en was nie verder ontwikkel nie.



Acknowledgements

I would like to express gratitude to the following people and organisations who have contributed to making this work possible:

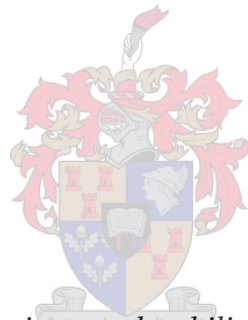
Firstly, I would like to thank Prof. van Niekerk for his excellent leadership, advice and challenging questions throughout the project, as well as the space to make this project my own. Dr Günther Migeotte at CAE Marine provided the enthusiasm which initiated this project, and gave valuable practical guidance throughout in all marine engineering and tank testing matters. Thanks must also go to the NRF for a generous grant for this project.

For help in designing and building the control mechanism, as well as being willing to modify parts on often short notice, the SMD personnel must be thanked.

Fanus Groenewald and Jakob Venter deserve special mention for building the servo controller, which worked perfectly throughout the project. All along, they provided huge amounts of practical know-how, greatly simplifying the implementation of the controller. Thanks for all the late night chats at the residence, where many ideas were discussed. Also, the system identification work would not have been possible without Keith Browne's interest in this work and his help, often even before I asked for it.

Jaco Kirstein also deserves mention for working alongside me (literally) for most of the project, and always being willing to help and to encourage some mountain biking and running to relieve academic stress. Also, thanks for an *incredible* road trip in Europe this year - unforgettable!

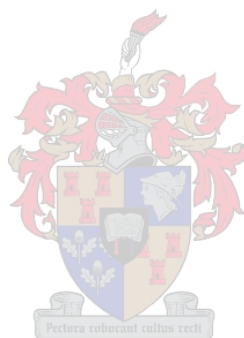
Dedication



*To the triune God who gives me the ability to do the things I love,
and the perseverance to do them well*

Contents

Declaration	i
Abstract	ii
Uittreksel	iv
Acknowledgements	vi
Dedication	vii
Contents	viii
List of Figures	xi
List of Tables	xiii
Nomenclature	xiv
1 Introduction	1
1.1 Motivation and background information	1
1.2 Objectives	2
1.3 Structure of this thesis	3
2 Literature review	4
2.1 Hydrofoils and catamarans	4
2.2 High speed ship theory	7
2.3 Planing	7



2.4	Ship seakeeping	9
2.5	Seakeeping calculation methods	10
2.6	Waves and seaway descriptions	12
2.7	Ride control systems	16
2.8	Conclusions	19
3	Potential-flow modelling of HYSUCATs	20
3.1	Two dimensional strip theory	21
3.2	Simulation inputs	23
3.3	Simulation tests	24
3.4	Comparison of simulation and experimental results	25
3.5	Discussion	29
3.6	Conclusions	30
4	State-space modelling of HYSUCATs	31
4.1	Two degree-of-freedom beam model	31
4.2	Modelling verification and tuning using system identification	34
5	Experimental validation	43
5.1	Experimental facilities used	44
5.2	Validation of POWERSEA simulations	48
5.3	System identification and control system validation	52
5.4	Experimental setup testing and error analysis	55
6	Control system design and implementation	58
6.1	Model summary for control application	58
6.2	Controller types and strategies	60
6.3	Control implementation results	64
6.4	Discussion and conclusions	70
7	Conclusions	74
7.1	Further work	75
	Bibliography	77

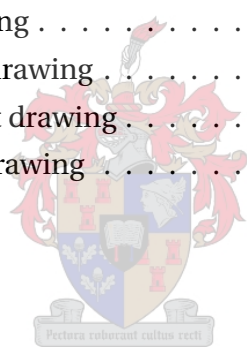
<i>CONTENTS</i>	x
Appendices	1
A Model HYSUCAT measurement and POWERSEA settings	2
A.1 Hull form measurement and simplification	2
A.2 Model parameter experiments	4
A.3 POWERSEA input settings	5
B Peter du Cane hydrofoil theory	7
B.1 Hydrofoil lift	7
B.2 Hydrofoil drag	7
B.3 Free-surface effects	8
B.4 Finite span effects	9
B.5 Planform, strut and geometry effects	10
B.6 Lift and drag summary	10
C Control mechanism drawings	12
D Servo drive user instructions	18



List of Figures

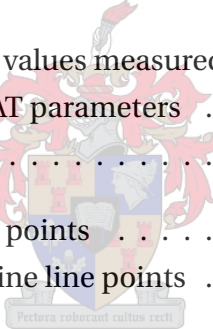
2.1	Typical HYSUCAT model application	6
3.1	Comparison of simulated heave RAOs to tank-test results	26
3.2	Comparison of simulated pitch RAOs to tank-test results	27
3.3	Measured model resistance	28
4.1	Linear two degree-of-freedom 'beam' model	32
4.2	Typical input signal used for system identification	35
4.3	Example of good parameter estimation result.	38
4.4	Large amplitude parameter estimation result.	39
4.5	Estimated heave damping parameter c_{ζ}	40
4.6	Estimated pitch damping parameter c_{θ}	40
4.7	Estimated heave spring stiffness parameter k_{ζ}	41
4.8	Estimated pitch spring stiffness parameter k_{θ}	41
5.1	The towing tank, along with the trolley used in testing	44
5.2	Load cell and sling towing arrangement	45
5.3	Trim sensor used to measure displacement of the model's bow and stern	46
5.4	Model HYSUCAT used in this study	47
5.5	The towing tank wave generator	49
5.6	Measured wave amplitude vs wave generation frequency	50
5.7	The trim foil control mechanism at the stern of the model	53
5.8	Schematic layout of experimental system	55
6.1	Controlled heave RAO comparison for initial three strategies, 4 m/s	66

6.2	Controlled pitch RAO comparison for initial three strategies, 4 m/s	66
6.3	Controlled heave RAO comparison for initial three strategies, 5 m/s	67
6.4	Controlled pitch RAO comparison for initial three strategies, 5 m/s	67
6.5	Controlled heave RAO comparison for initial three strategies, 6 m/s	68
6.6	Controlled pitch RAO comparison for initial three strategies, 6 m/s	68
6.7	Added resistance fraction due to waves for initial three control strategies at 4,5, and 6 m/s	69
6.8	Bow vertical position responses for all five control strategies tested	71
6.9	Stern vertical position responses for all five control strategies tested	71
6.10	Bow acceleration responses for all five control strategies tested . .	72
6.11	Stern acceleration responses for all five control strategies tested . .	72
C.1	Isometric view of mechanism assembly	13
C.2	Hinged hydrofoil drawing	14
C.3	Hydrofoil control arm drawing	15
C.4	Hydrofoil hinge bracket drawing	16
C.5	Hydrofoil control rod drawing	17



List of Tables

3.1	Measured model parameters for POWERSEA input	23
3.2	Measured hydrofoil parameters for POWERSEA input	24
4.1	Parameter values estimated from system identification results . . .	42
4.2	Vibration analysis results	42
5.1	Sensor specifications and values measured	44
5.2	Measured model HYSUCAT parameters	47
5.3	Servo specifications	54
A.1	Measured model keel line points	3
A.2	Measured model main chine line points	3



Nomenclature

Constants:

g 9,81 m/s²

i $\sqrt{-1}$

Variables:

A, B, C, D State space matrices

a, b, c Equation of motion coefficients

b Submerged width of a strip in m

C_L Lift coefficient

C_B Buoyancy reduction coefficient

c Damping constant in N · s/m, wave celerity in m/s, Foil chord length in m

D Drag in N

F Force/Force vector in N

$F_{n\nabla}$ Froude number based on displacement

h Water depth, in m

I Vessel moment of inertia, in kg · m²

j Counter

\mathbf{K} Full state feedback gain vector

K Foil lift slope in N/°

k Spring constant in N/m, wave number in m⁻¹

L	Vessel waterline length in m, Lift force in N, General length in m
M	Moment/Moment vector in N · m
m	Vessel mass in kg
m'	Added mass in kg
\mathbf{Q}	Output weighting matrix
\mathbf{R}	Control signal weighting matrix
r_G	Pitch radius of gyration about CG in m
S	Surface area in m ²
T	Wave period in s, Thrust in N
t	Time in s
t_d	Time delay in s
U	Vessel velocity along its own baseline in m/s
u	Control input angle in °
V	Vessel forward velocity (x -coordinate) in m/s
v	Local velocity in m/s
\mathbf{x}	State vector
x, y, z	Coordinates

Greek symbols:

α	Angle of attack
α_0	Zero-lift angle of attack
Δ	Change in variable, Vessel displacement mass in kg
ζ	Heave in m, Damping ratio
θ	Pitch in rad
λ	Wavelength in m, System eigenvalue, Scaling factor
ξ	Coordinate parallel to vessel baseline
ρ	Density, in kg/m ³
σ	Variance

ϕ	Velocity potential
ω	Wave frequency, rad/s
ω_e	Encounter frequency in rad/s
ω_n	Natural frequency in rad/s

Other symbols:

∇	Vessel volume of displacement in m ³
----------	---

Subscripts:

a	Adiabatic
a	Coordinate
B	Buoyancy
b	Bow
CG	Centre of gravity
D	Friction drag
e	Input
f	Main foil
i	Incident
N	Hydrodynamic normal
0	Equilibrium condition
s	Stern

**Abbreviations:**

CG	Center of Gravity
d.o.f.	Degree-of-freedom
HSST	High Speed Strip Theory
HYSUCAT	HYdrofoil SUpported CATamaran
LTI	Linear Time-Invariant
MII	Motion induced interruptions
RANSE	Reynolds-Averaged Navier-Stokes Equations

RAO	Response Amplitude Operator
rms	Root mean squared



Chapter 1

Introduction

1.1 Motivation and background information

As customers demand improved comfort, higher speeds and reduced costs from marine vessels, it has become increasingly important to understand and design for their seakeeping. Especially for vessels relying on passengers' comfort for their income, this continues to be an active and important area of research.

Significant benefits are to be gained from effective modelling and design for seakeeping. Some of these are: improved passenger comfort and satisfaction, reduced vibration-induced wear, improved crew performance, increased safety and (often) improved fuel efficiency. However, the complexity of the problem, especially in heavy seas, makes detailed analysis difficult. As explained by Bertorello (2001),

"... any type of HSC (High Speed Craft) for passenger transportation has, generally, very high accommodation and comfort standards which have to be maintained as far as possible in any weather condition. These requests force designers and ship owners to deal with the seakeeping of such crafts. At the moment the motion and pressure field prediction of modern hull forms at high speed is one of the most challenging tasks for the research in the marine field."

Highly non-linear seakeeping effects such as slamming and deck wash are almost impossible to simulate with current models and technology. Recent advances in these areas have been achieved by researchers such as Kihara (2004) and Constantinescu (2004), but solutions are typically only for simplified cases. For most practical applications, designers resort to semi-empirical potential flow models, especially 2- or $2\frac{1}{2}$ -degree strip methods. These focus on the 'vertical' motions of the vessel (pitch and heave). The POWERSEA computer program used in this study calculates vertical motions of a hard-chine planing vessel using strip theory developed by Zarnick (1978).

This thesis focuses on improving seakeeping of a specific type of hybrid multihulls known as HYdrofoil SUpported CATamarans (HYSUCATs). Much work has been done on this type of vessel regarding resistance, propulsion and stability, but thus far only Pienaar & Roos (1991) have considered seakeeping of these vessels. This, however, was an introductory study and no consideration was given to improving the model's motions.

Mechanisms improving seakeeping of a vessel can be active or passive. Modern electronics allows high-speed active control strategies to be implemented in real-time on a vessel. In this thesis, such a system will be designed to improve the seakeeping performance of a HYSUCAT using the motivation developed during the modelling process. Because of the aforementioned difficulties in modelling, a strongly experimental approach will be used to develop a *practical and reproducible* method of reducing the motions of a vessel. This is to be done using a representative HYSUCAT model as an example.

1.2 Objectives

The objectives of the current study are as follows:

1. Study applicable literature, particularly focusing on already existing ride control systems using hydrofoils.
2. Model the uncontrolled HYSUCAT vessel and its foils in regular sea states using POWERSEA, and determine the frequency responses, or Response Amplitude Operators (RAOs) for the vertical motions of the vessel.

3. Verify the seakeeping RAOs of the model using towing tank tests.
4. Obtain an appropriate linearised model to approximate the vessel's non-linear response.
5. Ascertain the validity of the above model by performing tests in the towing tank, and refine/change the model as necessary.
6. Design and implement an appropriate control system to improve the seakeeping of the vessel, particularly focusing on increased passenger comfort.

1.3 Structure of this thesis

The thesis is structured as follows: hydrodynamic modelling of a typical HYSU-CAT with fixed foils in regular waves is first given in chapter 3, including experimental validation of the results. This is followed by chapter 4, in which a state-space model of the vessel is presented and verified in smooth water. The model is then used in chapter 6 to design applicable nonlinear bang-bang as well as linear full-state-feedback controllers. Chapter 5 is a summary of the equipment and methods used in the experimental work.

In the appendices, the measuring of the model and POWERSEA inputs are described in appendix A. The empirical Peter du Cane theory for hydrofoil lift and drag is given in appendix B for reference. This is followed by the control mechanism drawings and servo driver circuit diagram in Appendices C and D, respectively.

Chapter 2

Literature review

Due to this project's wide scope, the literature study was necessarily broad, and thus limited in detail. First, a brief description of the HYSUCAT technology and hydrofoil calculations is given. This is followed by relevant topics in high-speed ship theory, particularly planing and seakeeping calculation methods for planing vessels. A brief description of the linear theory of ocean waves is given, and the chapter is concluded with a review of modelling and design of several ride control strategies and their application to practical vessels.



2.1 Hydrofoils and catamarans

A planing vessel is one in which a significant portion of its lift is from hydrodynamic forces generated by its forward speed. This acts alongside hydrostatic buoyancy to support the vessel. The lift provided by planing can be augmented by the use of hydrofoils, which provide added lift based on their profile and angle of attack. These are mature technologies and have been used extensively on vessels in the past century. The main advantages of a hydrofoil craft over a conventional planing craft are:

- Dramatically reduced hydrodynamic form (wave making) and skin friction drag due to the vessel being lifted out of the water,
- Improved fuel consumption because of this reduction in drag,

- Increased load-carrying capacity and
- Improved seakeeping due to the damping by the foils of vertical motions, as well as due to lower excitation forces between the ship's hull and the seaway.

The two main types of hydrofoil configurations are fully-submerged or surface-piercing hydrofoils. A good overview of configurations used is given by van Walree (1999). Surface-piercing designs enjoyed much popularity in the past, because they are self-regulating and do not require a control system to remain stable. However, they are gradually being replaced by more efficient, fully-submerged hydrofoils. A significant disadvantage of these, though, is that they require better design and a control system, as they become increasingly unstable as the foils support more of the vessel's weight.

As an example of fully-submerged foils, the 'tandem' configuration is often used, with approximately equal lift loads and sizing of the fore and aft foils. In the foil-borne mode, the system's stability is a major design concern. Matveev & Matveev (2000) give conditions for favourable applicability of this configuration, a comparison of vessels using it and the conditions for stability of the system.

In this project, a fully-submerged foil configuration is investigated, namely the patented HYSUCAT design. A picture of a typical application is given below in figure 2.1. It is a foil-assisted catamaran design, in contrast to a fully foil-supported catamaran where the vessel hull is clear of the water. In the HYSUCAT a large foil is situated close to the centre of gravity of the vessel between the two hulls, with small trim foils at the stern of the vessel. The main foil provides the primary lifting force to raise the vessel partially out of the water, and the trim foils provide the desired trim and increase stability, especially at high speeds. As well as increasing stability, keeping the vessel hull in water contact makes the propulsion of the vessel significantly easier.

The HYSUCAT configuration is thus a hybrid design between the traditional catamaran and the fully-supported foil vessel. It has many of the advantages mentioned above for a fully-supported vessel, without the need for



Figure 2.1: Typical HYSUCAT model application

a complex control system to maintain stability. The following is a description of modelling of the foils of such a vessel.

2.1.1 Hydrofoil calculations

For detailed hydrofoil calculations, especially in unsteady flow, the flow and pressures around the profile are required. However, for the purposes of the current project and in the interest of obtaining workable results as soon as possible, only the overall lift and drag of the foil are of interest. For more information on detailed foil calculations, see for example van Walree (1999).

In calculating lift and drag for a hydrofoil many factors affect the forces produced. Except for the free-surface effect of the water, techniques are very similar to those used in aerodynamics. The two-dimensional lift and drag of the profile are first calculated, and then adjusted using factors for the foil layout and three-dimensional flow effects.

These effects are collected by du Cane (1972) in an experimentally-backed hydrofoil theory, taking into account effects of foil ends, struts and variation of lift with submersion. Skin friction and profile drag components are accounted for empirically. A summary of the method is provided in appendix B.

Elements of the above theory are used widely in the literature, for example Arri (1993) and the POWERSEA program used in this project, which provides a modification of the strip theory described in section 3.1.

2.2 High speed ship theory

In the design of a high speed planing vessels, such as the HYSUCAT, the following design tasks are typically performed:

1. The *lift and drag* of the vessel at a certain speed must be determined to assess powering requirements and load capacity. This is usually dealt with using high-speed planing theory. If hydrofoils are present, this is coupled with a hydrofoil theory. A further description of planing theory is given in section 2.3.
2. The *seakeeping* of the planing vessel must be considered. This is the focus of the thesis, and is dealt with in section 2.4 below.
3. The *manoeuvrability* of the vessel needs to be determined. This includes study of the stability of the vessel in turning, the ability of the vessel to stop in an emergency and the vessel's ability to maneuver in tight spaces.
4. The *dynamic stability* of the vessel must be determined. This is in contrast to static stability, which is dealt with in hydrostatics. The dynamic stability of a vessel includes topics such as helming stability, porpoising and stability in maneuvers.

Of the above, this thesis uses planing and hydrofoil theory in its study of the seakeeping of a vessel.

2.3 Planing

Planing theory for high speed vessels gives an important basis for seakeeping calculations. The empirical concept of added mass, in particular, used extensively in planing theory, is also used in strip theory described below.

As is commonly seen, both theoretical and empirical approaches have been used to calculate planing lift and drag. Payne (1988) gives a good overview of the subject from both points of view, described below in more detail.

2.3.1 Classical planing theory

The theoretical ('classical') approach, starting in the early 1930's, was given attention by mathematicians when success was being had with similar approaches in aerodynamics. Wagner (1932) developed theory of lift and drag on two-dimensional plates using potential flow theory. These results of these analyses were recalculated by later researchers, which showed reasonably good agreement with experimental results. These methods were subsequently developed further to deal with three-dimensional problems.

2.3.2 Added mass planing theory

Added mass planing theory calculates lift and drag on a vessel moving at planing speed through calm water, and is based on the empirical idea of 'added mass'. This is an important concept used in a variety of applications involving motion of rigid bodies in high density fluids, such as vessels in water. It is used in manoeuvring, seakeeping and planing calculations, and greatly simplifies analysis without too great a sacrifice of accuracy in the answers obtained.

In principle, added mass theory treats the resistance to acceleration of a body accelerating in a fluid as an increased mass of the body itself. Thus Newton's second law is modified to

$$\mathbf{F} = \frac{d}{dt} [(m + m')\mathbf{v}], \quad (2.3.1)$$

where \mathbf{F} is the resultant force vector, m is the mass of the body, \mathbf{v} is the velocity of the rigid body and m' is the added mass of the body.

The amount of added mass varies according to the shape and size of the body. The most common of these is for a flat plate moving perpendicular to its own plane, where the added mass per unit length is given by $m' = \rho\pi y^2$ for a plate of width $2y$. Many experimental results have been condensed into empirical tables for other shapes, most commonly given as coefficients depending on the shape of the body. Payne (1988) gives these for many common body shapes, which are updated and further compared to extensive experimental results in Payne (1995).

The added mass is used in planing theory to describe the impact-like motion of the vessel hull into the water when viewed from a water-fixed reference frame. This accounts for the added lift experienced by a boat moving through the water. Other forces such as dynamic suction, transom drag and impact, among others, are each modelled independently, and their effect combined to determine the vessel's response. However, these are not used in seakeeping calculations, and are thus beyond the scope of this project.

2.4 Ship seakeeping

During a vessel's design, ship seakeeping calculations have historically been relegated to a fairly late stage of the process with tonnage, resistance and manufacturing considerations taking preference. However, as increased computation power allows quicker seakeeping calculations and clients demand ever more comfortable rides, these calculations have increased in importance.

Seakeeping of ships can generally be defined as the *calculation of added loads and/or motions of a vessel as a result of waves*. These have an impact on a variety of issues:

- Voluntary or involuntary reduction of speed because of the seaway, as well as risk of propeller race due to surfacing.
- Structural design of the ship for the expected loads. Reduction of wave loads reduces both fatigue and overloading failures, improving safety and cutting repair costs. However, predicting these loads involves time-integration of the pressure distribution on the hull, requiring detailed potential-flow or CFD calculations. Thus they are not commonly performed for commercial projects - the typical approach is to design to classification society standards, and then to monitor strains where necessary with strain gauges.
- Human comfort and performance aboard ship, including seasickness incidence and crew performance. See section 2.6.1 for more details.

- Ship and human safety including risk of capsizing, slamming and deck wash, as well as risk of man overboard.

Of the above, this thesis investigates only the issue of human comfort and performance aboard ship, with focus on reducing motions which cause seasickness and fatigue of passengers and crew.

2.5 Seakeeping calculation methods

The calculation of loads and/or motions of a vessel in a seaway is complex, and often difficult to verify experimentally. Methods used range from 2-D strip methods which are quick and focus on global motions, to full Reynolds-Averaged Navier-Stokes Equations (RANSE) CFD, which give detailed pressure and free-surface results. The following sections give details of the methods in use, as well as their typical application.

2.5.1 Seakeeping fitness methods

During the concept design phase for a new vessel it is impossible to perform detailed seakeeping calculations, as the hull form has not been finalised. Thus comparative methods are used by interpolating or extrapolating from a systematic series of experimental data of tested designs. The number of design parameters is typically low, including block coefficient, length and other overall metrics. Typically research is done on a particular hull form series, where many models are tested and the results empirically correlated.

The seakeeping results most used are those giving the pitch, heave and roll Response Amplitude Operators (RAOs). RAOs are the normalised amplitude of a parameter over a frequency range, and indicate approximate natural frequencies and damping ratios. Also sometimes used are nonlinear results such as slamming impacts or deck-submergences-per-hour in a certain seaway.

Advantages of the above methods are that they are quick and provide seakeeping comparisons between competing design concepts. However, the results given are only limited to vessels falling within the applicable range of data. For foil-borne catamarans, typically the number of design variables is

too large to obtain usable data from this method. Because of this, seakeeping calculations for HYSUCATs are most often done on the specific design, methods for which are described in the following sections.

2.5.2 RANSE CFD

In principle, the problem of ship seakeeping can be fully described by the Navier-Stokes and Continuity Equations. However, with current technology, modelling of every turbulent flow detail in the ship's boundary layers and wake is not possible, nor is it necessary. The RANSE can be used, but at present are impractically costly for all but research projects of selected simplified problems (Bertram, 2000). If viscosity of the fluid is neglected, the RANSE simplify to the Euler equations, but these tend also to be too expensive in practice. Thus the majority of simulations assume the flow to be irrotational as well, yielding the much simpler potential flow equations.

2.5.3 Potential flow methods

As noted above, potential-flow methods tend to be the most used for seakeeping calculations in practice. Many different approaches have been used, varying in the way that they discretise the hull form (2-D, $2\frac{1}{2}$ -D or 3-D), their treatment of the boundary conditions and distribution of the potential-flow singularities that are used. Bertram (2000) gives a good overview of the methods in use, and Zhu & Katory (1998) give an example of a specific Green-Function Method being applied to a non-planing ship, with good results.

Of the potential-flow methods, strip methods are most used because they are quick, cheap, relatively easy to implement and flexible enough for a variety of hull forms. Because of symmetry and a large length-to-beam ratio, a boat can be regarded as a series of transverse sections. The flow can then be solved around each section, with appropriate boundary conditions from one section to the other. This concept has been widely exploited in seakeeping calculation methods, especially for planing hulls, and two main approaches have been used:

1. The 2-D approach treats each cross-section as a separate entity, without direct interaction with other cross-sections. This is the method implemented in the POWERSEA program used in this thesis, and further information is given in section 3.1.
2. $2\frac{1}{2}$ -D Methods, often referred to as High Speed Strip Theory (HSST) are an improvement on the above, and include the effects of the upstream sections on a particular section. Ma *et al.* (2004) give an application of a $2\frac{1}{2}$ -D method, comparing the calculated coefficients of the system differential equations to experimentally-determined coefficients, showing how HSST is significantly better than 2-D methods at high speeds.

All of the above methods need some description of the waves that the vessel experiences, models of which are provided in the next section.

2.6 Waves and seaway descriptions

The mathematical description of ocean waves is important in any seakeeping study. For calculation purposes, linear theory is most often used, and gives reasonable results for small waves. Faltinsen (1990) gives the derivation of this linear ('Airy') theory from the inviscid, irrotational and incompressible Navier-Stokes Equations. Only the pertinent results will be given here.

Airy waves are inviscid and have a sinusoidal profile of a certain frequency, ω . They are affected by the average water depth, h , but the towing tank is deep enough (2,3 m) that this is not applicable in the tests to be performed. Thus the following results are all for water of 'infinite' depth. If needed, shallow water results can be obtained in Faltinsen (1990) or Bertram (2000).

The velocity potential, ϕ , is described by

$$\phi = \Re\left(-ic\hat{h}e^{-kz}e^{i(\omega t-kx)}\right) \quad (2.6.1)$$

for deep water, using the standard coordinate system. The velocities in the x and z directions are the partial derivatives in the respective directions as

follows:

$$v_x = \frac{\partial \phi}{\partial x} = \phi_x = \Re \left(-\omega \hat{h} e^{-kz} e^{i(\omega t - kx)} \right) \quad (2.6.2)$$

$$v_z = \frac{\partial \phi}{\partial z} = \phi_z = \Re \left(-\omega \hat{h} e^{-kz} e^{i(\omega t - kx)} \right) \quad (2.6.3)$$

Elementary waves are described by their wavelength λ , celerity (velocity) c , frequency ω and amplitude h . They are related by the following:

$$k = \frac{\omega^2}{g}, \quad (2.6.4)$$

where $k = 2\pi/\lambda$ is the 'wave number' and $g = 9,81 \text{ m/s}^2$. The celerity is the speed of an individual trough or crest, and is given by

$$c = \sqrt{\frac{g}{k}} = \frac{g}{\omega} = \frac{gT}{2\pi} \quad (2.6.5)$$

From a single wave height sensor, the frequency and amplitude of a wave can be determined. However, this is not enough to measure the celerity and/or wavelength of the wave directly, and thus these must be calculated using equations 2.6.4 and 2.6.5 above. If two wave height sensors are available, they can be spaced a fixed distance in the direction of the wave travel, and the relationships above can be verified. However, this was not possible in the available experimental setup.

2.6.1 Desired motions/seasickness measurement

In designing a ride control system for a particular goal, it is important to be able to quantify the vessel's motions and their effect, and focus improvement efforts on the primary sources of the problem. Primary 'human factor' reasons to control a vessel's motions are:

1. Reduction in motion sickness among passengers and crew aboard passenger vessels. This effect is discussed below in more detail.
2. Reduction of motion induced interruptions in crew work, thus increasing crew performance. This is typically due to the need to brace oneself,

and thus stop working, when heavy motions are encountered. A probability of Motion-Induced Interruptions (MII) or 'loss-of-balance events' (Lewis and Griffin, 1997) is used to quantify the amount of crew performance lost due to the motions.

3. Reduction in fatigue of passengers and crew due to constant physical compensation for the vessel's motions. This is particularly important for high-use vessels such as patrol and fishing boats.

These items are closely related, as an improvement in one will generally cause an improvement in the others as well. This human factor usually is the overriding concern in seakeeping reduction, as *very often, the speed of a fast ship is limited by the human element, i.e. the passengers' or crew's ability to cope with the motions*. In this project, the focus is on seasickness as it is the most common problem caused by a vessel's motions, and it occurs at a frequency low enough that can practically be controlled.

The exact causes of seasickness, and motion sickness in general, is somewhat debated in literature. Griffin (1990) gives a good review of the literature pertaining to motion sickness and the current knowledge about it. It gives physiological explanations that are currently available, focussing on the effect of motions on the vestibular systems of the ear.

Despite the uncertainty in the cause of seasickness, the data obtained of the percentage of people experiencing seasickness is summarised in the Motion Sickness Incidence (MSI). The most well-known experimental work to determine the MSI curves was done by O'Hanlon & McCauley (1974), which concluded that motion sickness is primarily caused by accelerations in the vertical direction. The curves indicate that motion sickness is a statistical process caused by linear accelerations of the body in the frequency range of 0,1-0,5 Hz, with a maximum incidence at 0,2 Hz. It is a strongly time-dependent process, with increasing incidence over time.

The International Organisation for Standardisation (ISO) has compiled a standard for motion sickness, 2631-1, to aid in design to for this effect (ISO, 1997). The frequency-weighted linear acceleration rms value is multiplied by the exposure time to obtain an acceleration 'dosage'. This is then correlated to

the MSI percentages. Generally accelerations used are the values at a certain location on the vessel, often the centre of gravity and/or the forward point. This is useful, but can be improved by considering the maximum MSI occurring over the length of the vessel. This ensures that a 'worst-case scenario' is taken into account, and provides a single metric, making comparison easier.

That only linear accelerations contribute to the above is the most common assumption, but it has been questioned more recently by Wertheim *et al.* (1999), who investigated the effect of pitch and roll motions on seasickness. In this study, a significant proportion of subjects became motion-sick when exposed to purely pitch and/or roll motions, and this should be investigated further for inclusion in current models.

2.6.2 Passive motion damping systems

The above motion effects are controlled in a variety of ways. These can be divided into *active* and *passive* systems. Active ride control systems are the main focus of this project, and are considered in depth in section 2.7 below.

Regarding passive systems, there is evidence indicating that some form of damping by means of stationary foils/fins can significantly improve vertical motions without sacrificing much in the way of added resistance. Welnicki (1998*a*) and Welnicki (1998*b*) describe experimental investigation into the effect of variation in

- A single foil between the hulls of a fast catamaran at 3 longitudinal positions;
- T-foils at the bows of the catamaran;
- Variation in angle of attack of the above foils.

Conclusions from this research were that the full foil had better overall motion reduction than the T-foils at the bow, and that a position 0 – 25% of waterline length from the bow was the most effective location for the foil. Reductions in motions for this location were 20 – 75% for the peak accelerations at the forward point and centre of gravity of the model. Static variation of angle of

attack did not effect motions much; the angle $\alpha_i = 0$ seemed best. Added resistance for this configuration was 10 – 19%, indicating the cost in powering for these reductions in motions. Therefore this approach can be considered in a design if a simple damping in motions is required, but at the cost of extra power.

2.7 Ride control systems

The design of ride control systems for vessels in practice varies widely, with almost as many approaches as designers. However, the process can usually be divided into three phases. The first is the modelling of the system, as done in section 2.7.1 below. This is followed by the hardware and algorithm design for a control system, often in tandem with the physical layout of the control on the vessel itself. Example algorithms are given in section 2.7.3. Finally, the hardware and software must be installed and tested on board the vessel.

2.7.1 Vessel modelling

In order to be able to design a control system for the particular vessel, an appropriate model of its response must first be formulated. Because ship sea-keeping is significantly nonlinear, this can be a difficult task. Most approaches linearise the modelled or experimentally-determined system equations about some operating point, and then either use gain scheduling or some heuristic nonlinear model to describe deviations from it. The parameters used can then be estimated using excitation experiments and/or seakeeping simulations described in section 2.5 above.

The linearised differential equations of motion for a ocean vessel are given in various literature. Bertram (2000) gives the final equations in summary, while a very comprehensive description of their derivation is given by Fossen (1994). Most researchers use a simplification of the 6-d.o.f. Euler equations for a rigid body. These are split up between vertical motions (heave, pitch and surge) and lateral motions (yaw, sway/drift and roll). In vertical motions,

surge is often ignored, and for horizontal motions, often roll is treated separately from yaw and sway.

For the pitch and heave motions, the typical representation is as given in Haddara & Xu (1997), where the motions are described by two linear second-order ordinary coupled differential equations in the following form:

$$\begin{aligned} \begin{bmatrix} (m + a_{33}) & a_{35} \\ a_{53} & (I_{55} + a_{55}) \end{bmatrix} \begin{bmatrix} \ddot{x}_3 \\ \ddot{x}_5 \end{bmatrix} + \begin{bmatrix} b_{33} & b_{35} \\ b_{53} & b_{55} \end{bmatrix} \begin{bmatrix} \dot{x}_3 \\ \dot{x}_5 \end{bmatrix} + \\ + \begin{bmatrix} c_{33} & c_{35} \\ c_{53} & c_{55} \end{bmatrix} \begin{bmatrix} x_3 \\ x_5 \end{bmatrix} = \begin{bmatrix} f_3(t) \\ f_5(t) \end{bmatrix} \end{aligned} \quad (2.7.1)$$

where m is the mass of the ship, and I_{55} is the moment of inertia of the ship about a horizontal axis passing through the centre of gravity of the ship. a_{ij} , b_{ij} , c_{ij} , $i, j = 3, 5$, are the added mass and added moment of inertia, the damping coefficients and the restoring force and moment in heave and pitch, respectively. $f_3(t)$ and $f_5(t)$ are the exciting force and moment in heave and pitch, respectively.

The above model is not particularly intended for hydrofoil craft, so it must be modified for the hydrofoil configuration used. As the above model is linear, the linear lift equation of foil lift, given by

$$L = \rho S V^2 \frac{dC_L}{d\alpha} \alpha \quad (2.7.2)$$

is often used in a superposition of forces. The variation of lift with depth is sometimes omitted for the sake of linearity, though it is included by du Cane (1972), given in appendix B. A limitation of this model is due to the fact that interaction effects between the foils and hull are omitted.

For fully foil-supported craft, the equations are greatly simplified due to the absence of hull effects. Kim & Yamato (2003) give equations of motion and their derivation for a fully-submerged hydrofoil craft, especially considering the added effect that the orbital wave velocity has on foil lift. This effect is noticeable in waves, and makes modelling considerably more difficult.

2.7.2 System identification and parameter estimation

Many difficulties have been experienced in modelling high speed vessels in waves (especially with foils) when combining elements by linear superposition. Because of this, various ingenious approaches have been implemented in recent years to provide experimentally-based and workable models. These have primarily been implemented to improve the robustness of the controller designed.

Santos *et al.* (2004) used existing data from a model and linear simulation program to design a neuro-fuzzy model of the vessel. The inputs to the model are a) the Sea State Number given by ω_0 or the wavelength, b) the ship speed and c) the ship heading relative to the waves. The outputs given are heave and pitch amplitude and phase, as well as pitch moment. This model is much more robust than any single model formulated at a particular operating point, and is used with a PID controller to give the control signals. Experimental improvements quoted for pitch rms accelerations are between 26 and 65%.

A different approach was used by Haddara & Xu (1997), where neural networks are used for a combination of parameter estimation and system identification. The linear coupled differential equations for pitch and heave (See section 2.7.1) are assumed with unknown coefficients, and the coefficients describing the nonlinearity are lumped together in a separate function. The form of this nonlinear function is not assumed a priori, but a Markov process theory approach was used with random decrement functions to determine its form. Random decrement results were calculated with this method, and compared to experimental data, which shows good results when the system is lightly damped.

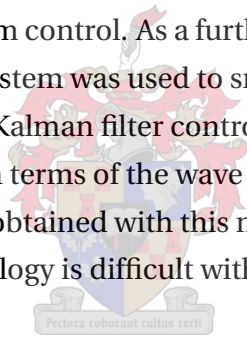
2.7.3 Algorithms

As mentioned above, many different control design strategies are used in the literature. These range from the most basic PID control strategies to an 'optimal preview' system, where a forward-looking predictive control strategy is used. Below are some of the strategies being used. Here, only those relating to

control of vertical motions are dealt with. The results quoted cannot be easily compared, as each method used was different.

Bhardwaj (2004) designed a control system for the vertical motions of a model boat using the trim tabs on the vessel's stern. Very little attention is given to system modelling, and the primary work is experimental. The only control strategy used is that of a 'bang-bang' control of the trim tabs based on the pitch velocity, i.e. a positive pitch velocity caused the trim tabs to instantaneously lower, and vice versa. Quantification of the results was by the RAOs of the without- and with-control situations. The RAO was compared to a standard 2nd-order system frequency response, and a damping coefficient was obtained and compared to it.

Kim & Yamato (2004) used a Kalman filter to estimate a vessel's motion and compensate for sensor and state noise. This helps to filter out the effects of the sensor noise on the system control. As a further improvement, a 'forward-looking' predictive control system was used to smooth vertical motions of the vessel. This is an optimal or Kalman filter control design, but with an estimation of the upcoming wave in terms of the wave experienced up to that point. Generally good results were obtained with this method, and it seems that improvement of current technology is difficult without such a 'forward-looking' system.



2.8 Conclusions

This literature study outlines the background information used in understanding the vertical motions of a HYSUCAT in waves, as well as means to control these motions. It further supports the idea that there is scope for reduction of these motions using simple methods. Modelling of the system is now given in the following two chapters, in order to understand it well enough to control the motions.

Chapter 3

Potential-flow modelling of HYSUCATs

In order to predict the motions of the model boat in waves, it was necessary to simulate the experimental setup. This was done with a two-dimensional strip theory program POWERSEA®, which is proprietary software of Ship Motion Associates, Inc. (www.shipmotion.com).

POWERSEA uses a modification of the strip theory given by Zarnick (1978). It divides the vessel into lateral 'slices' perpendicular to the motion of the vessel. For each of these, the force experienced by the hull 'strip' is calculated using inviscid potential flow theory. The strips are coupled, and the simulated waves are moved backwards along the hull as the vessel moves forward. To solve the problem of the viscous flow found behind the bluff transom and chines, a 'dry transom and topsides' assumption is made. This means that the water leaves the boat at the lower stern edge and the chines, making the theory only applicable for planing high-speed vessels where this actually occurs. The resulting calculated accelerations are then integrated forward in time to obtain the motions of the vessel.

3.1 Two dimensional strip theory

The basic approach and equations of the strip theory used by POWERSEA is given here. The full theory is available in Zarnick (1978) and Akers (1998). The primary assumptions of the theory are as follows:

- The vessel has a single chine, and the hull surface between the chine and keel is flat and is the only section that is ever wetted;
- The vessel sections moving past a water-fixed reference point can be modelled as an impacting wedge;
- The normal forces experienced by an impacting wedge can be approximated using the added mass of the section;
- The wavelengths encountered will be large w.r.t. the vessel's length;
- The planing vessel has a dry transom (Kutta condition);
- Wave slopes are small and the wave velocity field can be approximated by linear wave theory.

If the equations of motion of a vessel are restricted to surge x_{CG} , heave ζ_{CG} and pitch θ , the equations of motion can be written as

$$\begin{aligned}
 m\ddot{x}_{CG} &= T_x - F_N \sin \theta - F_D \cos \theta \\
 m\ddot{\zeta}_{CG} &= T_\zeta - F_N \cos \theta + F_D \sin \theta + mg \\
 I\ddot{\theta} &= F_N x_c - F_D x_d + T x_p
 \end{aligned} \tag{3.1.1}$$

where

- m and I are the mass and moment of inertia of the vessel, respectively;
- F_N is the hydrodynamic normal force;
- F_D is the friction drag;
- T_x and T_ζ are the thrust components in the x and ζ directions, respectively;

- x_c , x_d and x_p are the moment arms for the normal centre of pressure, the friction drag and the thrust, respectively.

The differential hydrodynamic normal force dF_N contains a component proportional to the rate of change of momentum and a drag term, given by

$$dF_N = - \left(\frac{D}{Dt} (m'v) + C_{D,c} \rho b v^2 \right) \quad (3.1.2)$$

where $\frac{D}{Dt} (m'v) = m' \dot{v} + \dot{m}' v - U \frac{\partial}{\partial \xi} (m'v) \frac{d\xi}{dt}$

where U is the velocity normal to the baseline, m' is the added mass of the section, $C_{D,c}$ is the crossflow drag coefficient, ρ is the fluid density and b is the half beam.

In addition to the normal force on the section caused by its motion, it also experiences a differential buoyancy force dF_B , expressed by

$$dF_B = -C_B \rho g dS \quad (3.1.3)$$

where dS is the differential cross-sectional area of the section, and C_B is the factor indicating the reduction from static buoyancy caused by the motion of the boat (usually approximately 0,5).

Combined, the differential forces on each strip are integrated along the length of the hull to obtain the hydrodynamic forces for equation 3.1.1. Similarly, the force on each strip is multiplied by its moment arm and integrated to obtain the resultant moment. These are given by:

$$\begin{aligned} F_\zeta &= \int_L (-dF_N \cos \theta + \rho g C_B S) d\xi \\ F_x &= \int_L -dF_N \sin \theta d\xi \\ F_\theta &= \int_L (dF_N + \rho g C_B S \cos \theta) \xi d\xi \end{aligned} \quad (3.1.4)$$

These forces, along with the thrust, drag and weight forces, are substituted into equation 3.1.1 to get the overall force experienced by the vessel. This is then used to calculate the accelerations of the vessel, which are integrated

forward in time to obtain the vessel's motions.

3.2 Simulation inputs

POWERSEA uses the keel and chine lines to describe a hull. The physical hull was measured up, imported into the program, and smoothed in 3-D using a cubic spline. The points used are available in appendix A.1. The overall parameters such as mass, moment of inertia, etc. were also measured up, and are provided in table 3.1. The theory and methods used to obtain these values are given in appendix A.2.

Table 3.1: Measured model parameters for POWERSEA input

Measured parameter	Value
Propulsion position(towing point)	$x = -0,655 \text{ m}, z = 0,276 \text{ m}$
Centre of gravity (CG)	$x = -0,548 \text{ m}, z = 0,16 \text{ m}$
Mass	22,29 kg
Radius of Gyration at CG	0,402 m
Moment of inertia	3,602 kg · m ²

The description of the HYSUCAT's foils is implemented in POWERSEA using the Peter du Cane foil theory. To obtain the zero-lift angle of attack α_0 , a standard potential-flow integration over the (circular segment) profile was used, as given in Houghton & Carpenter (1993), giving $\alpha_0 = -3,854^\circ$. The geometric parameters describing the foils used is given in table 3.2.

Using the above parameters for vessel and foils, the setup was simulated in smooth water and regular waves of a range of frequencies. The POWERSEA settings used for the runs are given in appendix A.3.

Built into POWERSEA is the option to run a 'response' calculation for regular waves. This performs the same seakeeping calculation as above for a specified range of wavelengths, recording the heave and pitch amplitudes for each one. These can then be easily converted into an RAOs for the heave and pitch of the vessel, and was used in the results displayed below in section 3.4.

Table 3.2: Measured hydrofoil parameters for POWERSEA input

Measured parameter	Main Foil	Trim Foils (each)
Foil angle	0°	-1,7°
Horizontal loc. (fwd of stern)	0,545 m	$8,0 \times 10^{-3}$ m
Vertical loc. (above baseline)	6×10^{-3} m	20×10^{-3} m
Sweepback angle	25,21°	0°
Dihedral angle	0°	0°
Full width	0,26 m	70×10^{-3} m
Strut width	0,26 m	0 (disabled)
Foil thickness	$4,9 \times 10^{-3}$ m	$2,5 \times 10^{-3}$ m
Surface roughness	1×10^{-4} m	1×10^{-4} m
Chord length	$73,5 \times 10^{-3}$ m	45×10^{-3} m
C-Lift factor	1,0	1,0

3.3 Simulation tests

To provide improved confidence in the numerical fidelity of the results given by the POWERSEA program, several tests were performed.

Simulation tolerance test POWERSEA reduces the time step if the estimated error is greater than a specific tolerance. This value is made up of a fraction of the state variables given by a *relative tolerance*, as well as an *absolute tolerance* value for each state variable. In the *Analysis->Simulation Tolerances* settings, default tolerances give reliable convergence for most runs. For those that did not converge, however, reducing these values did not improve the situation at all. Thus these settings can be left at their default values as recommended in the user's manual.

Time step adjustment In order to reduce the amount of data generated by a small time step, identical simulations with varying time steps were superimposed. POWERSEA's automatically-generated time step was found to be shorter than necessary, and could be doubled without any noticeable effect on the results.

Variation of number of hydrodynamic sections POWERSEA is capable of simulating vessels with up to 301 transverse 'strips', but the default is set at 201, and was used throughout. Because the vessel is made up of very

simple curves, a much smaller number of sections is adequate to describe the hull, and the default number did not need to be increased. On the other hand, the simulations were also relatively quick (< 1min), so it was unnecessary to reduce the number for the sake of speed.

Test of 'Response' function vs individual runs To check that the built-in 'Response' function was producing expected results, several of the RAOs were built up from saving the results of individual runs. When plotted over the 'Response' results, they matched almost identically, showing that the methods used to calculate the automated RAOs are as expected.

3.4 Comparison of simulation and experimental results

The scope of the simulations was for a full scale $F_{nV} = V/\sqrt{g\nabla^{1/3}}$ of 2,2 - 5,0, which is the typical range of planing speeds. Using a displacement $\nabla = \Delta/\rho = 22,29/998 = 22,33 \times 10^{-3} \text{ m}^3$ gives a range of velocities of $V = 3,66\text{-}8,3 \text{ m/s}$. Thus speeds of 4, 5, 6 and 7 m/s were chosen for convenience. The choice of wave height was to cover the range of heights available in the towing tank; 3 heights were used, $A = 0,01 \text{ m}, 0,02 \text{ m}$ and $0,04 \text{ m}$.

Simulations were run for all combinations of the above frequencies, Froude numbers and wave heights. Experimental towing tank runs were then used to get the results experimentally. The theoretical RAOs of the POWERSEA simulations are compared to experimental results in figures 3.1 and 3.2, as well as the model resistances measured in figure 3.3. Only the post-processed results are given here; full details of the experimentation are provided in chapter 5. The heave RAOs are the ratio of heave amplitude to wave height $\zeta_{\text{rms}}/h_{\text{wave,rms}}$, and the pitch RAOs are the pitch angle amplitude over the wave number k and the wave height, $\theta_{\text{rms}}/(kh_{\text{wave,rms}})$. The expression $\omega_e\sqrt{L/g}$ is used to normalise the encounter frequency ω_e with length. Note that the experimental wave amplitudes produced by the wave generator are not directly controllable, and thus do not match the simulated amplitudes exactly. Experimental wave amplitudes vary from 0,015 - 0,04 m (see figure 5.6).

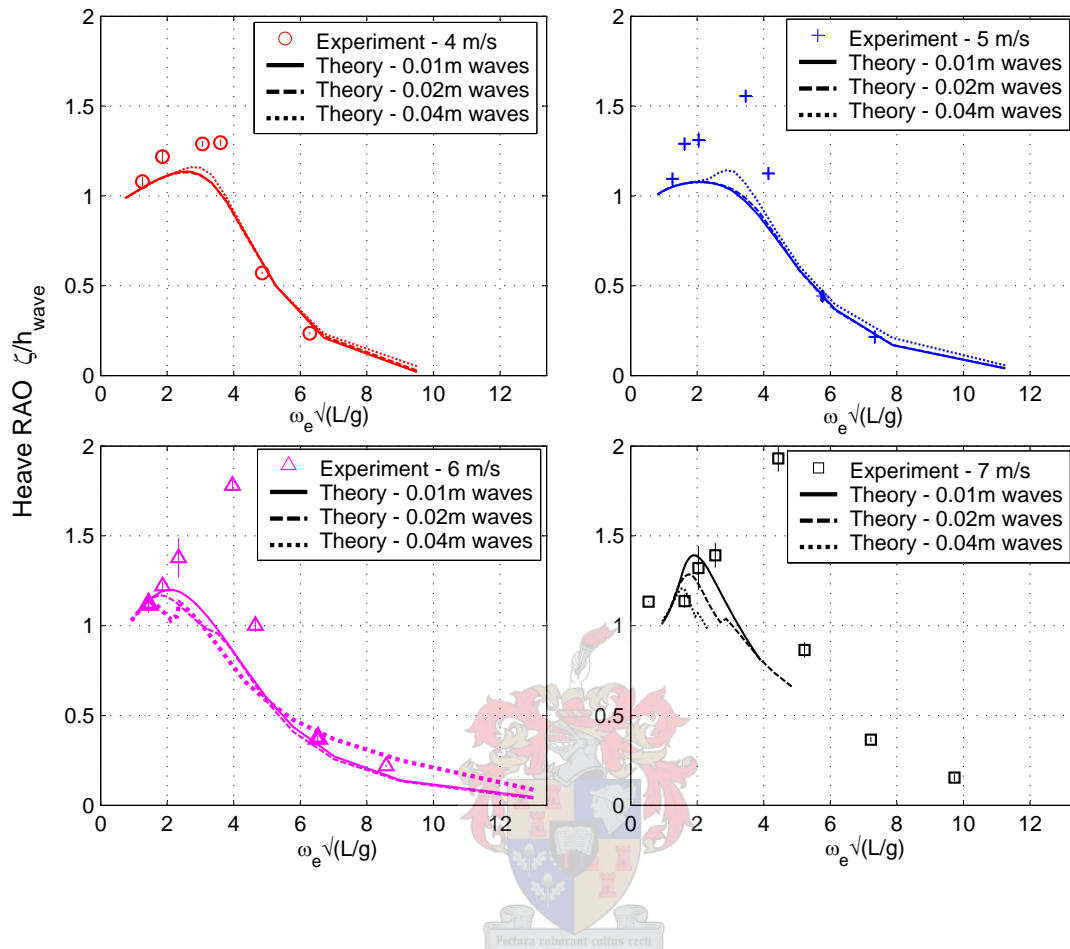


Figure 3.1: Comparison of simulated heave RAOs to tank-test results

The following properties of the results can be noted:

Linearity Because the RAOs presented are normalised by wave height, linear simulation results should lie on top of each other for all heights tested. This occurs at 4 m/s, but as the vessel speed increases, the match is not as close. This shows that POWERSEA is capturing some of the non-linear response characteristics of the vessel.

Convergence consistency Smooth simulation results were obtained for all wave heights at 4 and 5 m/s, but steps can be noted in the highest waves at 6 m/s and all but the lowest waves at 7 m/s. These steps are caused at frequencies above the natural frequency of the system, and it was found

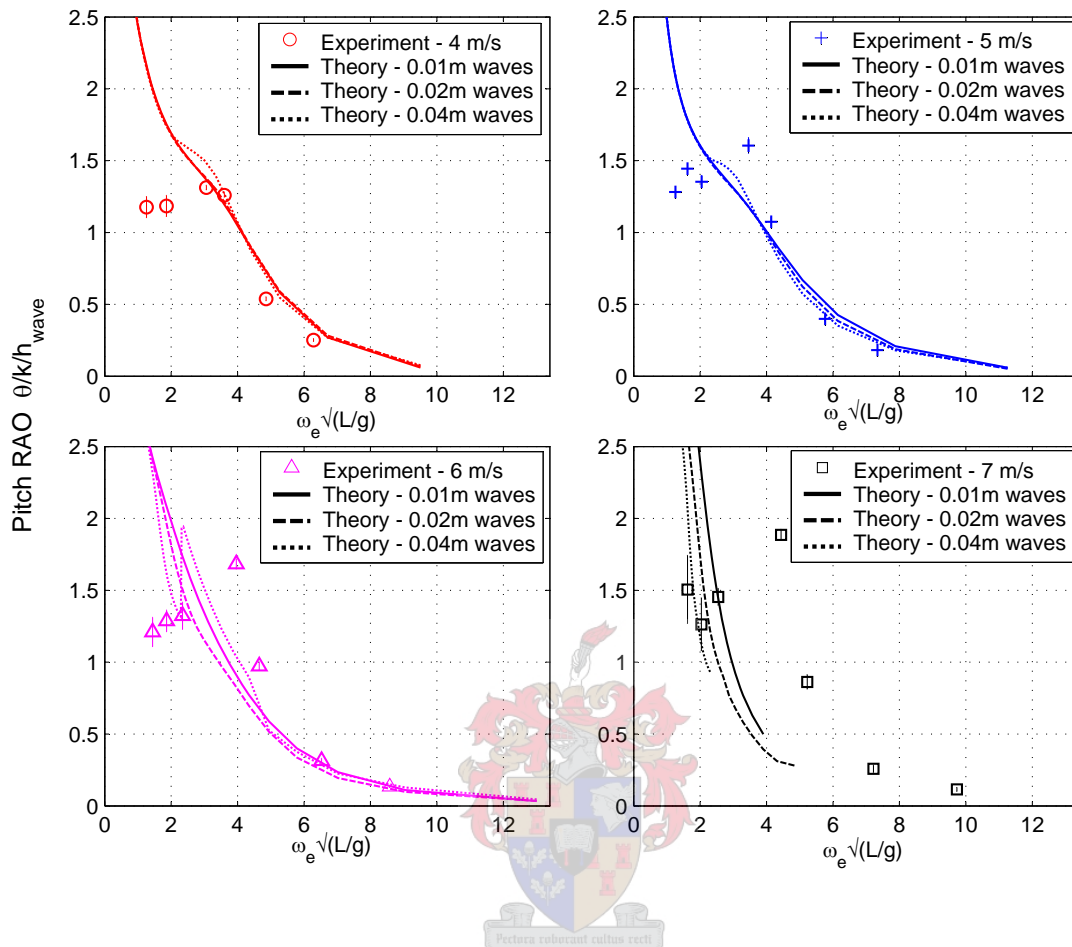


Figure 3.2: Comparison of simulated pitch RAOs to tank-test results

that the computation does not converge continuously at that frequency. Thus, for simulations at higher frequencies, the results are questionable.

Simulation extremes - heave response For the heave RAO, both the predicted and measured results tend to unity at low encounter frequencies, and to zero at high frequencies. This is to be expected because:

- At low frequencies, the wavelengths are long relative to the boat length. This means that the model moves with the waves, and the input and output heights will be equal;
- For high frequencies, the wavelengths are short relative to the boat length. Thus there is more than one wave experienced by the ves-

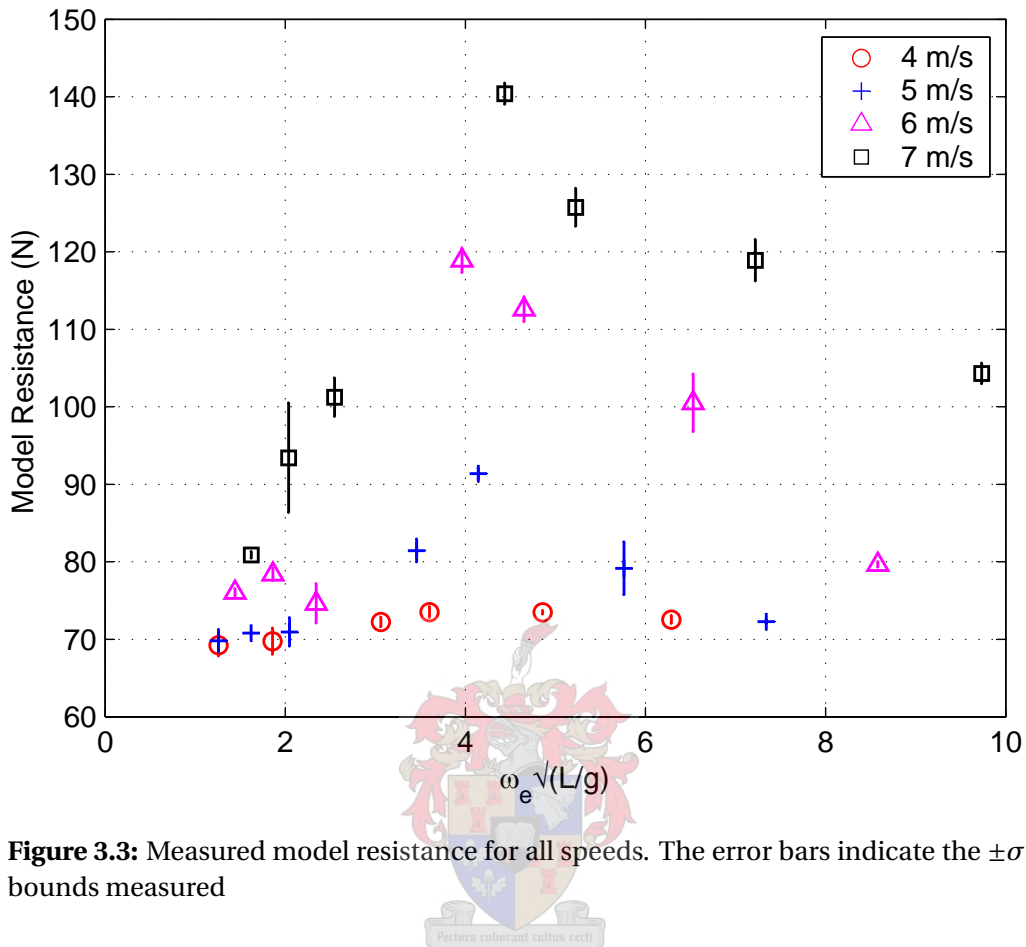


Figure 3.3: Measured model resistance for all speeds. The error bars indicate the $\pm\sigma$ bounds measured

sel simultaneously, and the heave motions will average these out and be equal to zero.

Simulation extremes - pitch response For the pitch RAO, the measured results have the same tendencies as for the heave results provided above. However, for the simulated results, while correctly tending to zero at high frequencies, the tendency at low frequencies is towards infinity. This is because the theoretical limit of the pitch RAO is $0/0$, can be ∞ if the denominator (wave number) tends towards zero faster than the numerator. See the discussion below for further details.

3.5 Discussion

From the results presented above, the following points are noted:

- The predicted peak produced in simulation is lower than the experimentally measured value. If the system is treated as a 2nd-order mass-spring-damper system, this means that the damping has been over estimated, smearing out the peak responses;
- The damped natural frequency of the system in heave and pitch is predicted well by the simulations at the low speeds of 4 and 5 m/s;
- The experimental pitch RAO is well predicted by the simulation at 4 m/s, taking into account the variation of wave heights given by the wave generator and the lack of agreement at low frequencies given below. However, the prediction of RAOs deteriorates rapidly as speed increases. By 7 m/s, neither the natural frequency location and amplitude are represented;
- The frequency predicted for the peak is represented well for 4 m/s, but deteriorates rapidly for higher speeds. At 7 m/s, the results are totally unrepresentative of the measured values, showing the limitation of the strip theory at higher speeds (see section 2.5.3 for further information on potential flow methods);
- The measured natural frequencies increase with increasing speed, showing how the vessel response stiffens at higher Froude numbers. This effect is further encouraged by the depth dependence of the foil lift, which is also greater at higher speeds.
- The low frequency results obtained, especially for the pitch RAOs, do not tend to the limiting value of 1. Problems with low frequency prediction from strip methods is noted both by Akers (1998) and Savitsky & Koelbel (1993). The reason for this seems largely to be due to the quotient of small numbers at this point, magnifying small numerical and modelling errors.

3.6 Conclusions

From the above, the POWERSEA simulations have been effective in predicting the trends of the vessel's heave response at low planing speeds. The peak response amplitude and frequency are under-predicted but otherwise the prediction is acceptable. As the vessel speed increases, though, the correlation deteriorates and cannot be used for prediction even for the system's natural frequency.

For the pitch RAOs, the theory provides acceptable correlation for low and medium planing speeds above the natural frequency. At higher speeds, and below the natural frequency, the results are not usable. However, this is expected as it is predicted by various literature sources, including the POWERSEA user's manual.

It was found that the disparities between POWERSEA simulations and experimental results are also exacerbated by the Peter du Cane hydrofoil model used. Reasons for this are:

- The foil theory used has been developed from steady state empirical models, and is primarily intended for steady-state calculations. Time-dependent foil models are not included to capture transient effects;
- Apart from the strut effects, the foil theory does not take the hull-foil interactions into account. For example, the hull shape could be deflecting the water and changing the foil's angle of attack. The POWERSEA program simply assumes the foil's angle of attack is based solely on the vessel's pitch angle, the angle of the foil and the circular velocity of the water in the waves;
- The POWERSEA program does not simulate the effect the main foil has on the stern trim foil. Various literature sources mentioned it as a possible shortcoming of their models, and included this effect empirically.

Based on the above, the planned implementation of a controllable foil in the POWERSEA model was not carried out; instead, a state space model of the system was proposed, and the parameters identified experimentally. This is given in chapter 4 which follows.

Chapter 4

State-space modelling of HYSUCATS

Chapter 3 presents modelling of the seakeeping of the HYSUCAT system using a potential-flow strip method. The simulation results obtained were not sufficiently accurate for the system's control design, motivating a more experimental approach to obtaining a system model.

4.1 Two degree-of-freedom beam model

In order to design a controller for the vessel, it is necessary to obtain a simplified model which captures the basic vessel dynamics. An HYSUCAT's motions are nonlinear, and detailed time-domain hydrodynamic modelling of the system would be necessary for accurate results. However, this is computationally extremely intensive as simulations must be performed in time using each individual control strategy and wave frequency distribution to be studied. Also, as can be seen from results given in section 3.4, the POWERSEA software used to model the system is not sufficiently accurate to provide reliable results for these kind of calculations, and a more advanced model would be needed.

Thus a linear time-invariant (LTI) model was proposed about the running trim of the vessel, linking up the physical dynamics of the system to various appropriate coefficients. This approach is common in the literature; see sec-

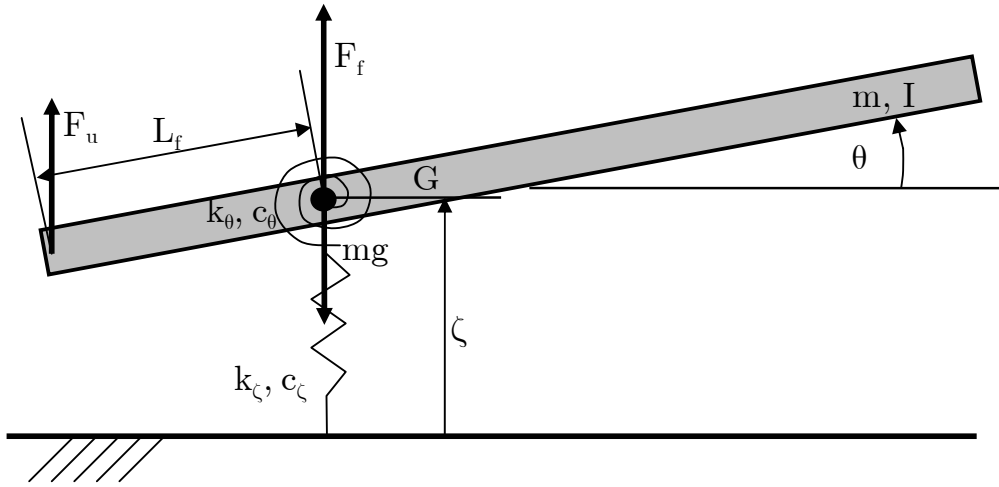


Figure 4.1: Linear two degree-of-freedom 'beam' model

tion 2.7.1 for more details.

The two degrees of freedom of the system require two variables. For each of these degrees of freedom, the system is treated as a second order mass-spring-damper system. The coupling between these is described below. Thus the full system can be described by a fourth order state-space system. These can be for example: pitch and heave at a certain point, height of the fore and aft points, or any other independent set. In this case, the heave ζ , and pitch θ at the centre of gravity of the vessel were chosen.

For derivation of the equations of motion of the system, the constants k_ζ , k_θ , c_ζ , c_θ as well as the mass m and moment of inertia I are assigned as shown in figure 4.1, a schematic diagram of the system. Modelling of the lift from each of the two foils is included in appendix B.

In the ζ direction, Newton's second law for constant m is

$$\sum F_\zeta = m\ddot{\zeta} \quad (4.1.1)$$

while in the θ direction, we have

$$\sum M_\theta = I\ddot{\theta}. \quad (4.1.2)$$

From the free body diagram, these become:

$$F_{k\zeta} + F_{c\zeta} + F_f + F_u - mg = m\ddot{\zeta} \quad \text{and} \quad (4.1.3)$$

$$M_{k\theta} + M_{c\theta} - F_u \cos\theta L_u = I\ddot{\theta}, \quad (4.1.4)$$

where ζ and θ are the heave and pitch variables, L_u is the distance from the control foil to the centre of gravity and F_f and F_u are, respectively, the lift forces due to the main foil and the controllable trim foil.

With linear relationships such as $F_k = k(x - x_0)$ and $F_c = c(\dot{x} - \dot{x}_0)$ for the spring and damper forces and using small angle approximations, the above become

$$-k_\zeta(\zeta - \zeta_0) - c_\zeta(\dot{\zeta} - \dot{\zeta}_0) + (F_{f0} + \Delta F_f) + (F_{u0} + \Delta F_u) - mg = m\ddot{\zeta} \quad (4.1.5)$$

$$-k_\theta(\theta - \theta_0) - c_\theta(\dot{\theta} - \dot{\theta}_0) - (F_{u0} + \Delta F_u)\theta L_u = I\ddot{\theta}, \quad (4.1.6)$$

where the subscript 0 indicates the steady-state running trim condition, and Δ indicates a change in value.

If equilibrium equations are subtracted from the above only the changes in variables remain, and dropping the Δ for brevity these become

$$\ddot{\zeta} = \left(\frac{1}{m}\right)[-k_\zeta\zeta - c_\zeta\dot{\zeta} + F_f + F_u] \quad \text{and} \quad (4.1.7)$$

$$\ddot{\theta} = \left(\frac{1}{I}\right)[-k_\theta\theta - c_\theta\dot{\theta} - F_u L_u] \quad (4.1.8)$$

The foil forces are made up of lift and drag. Only the lift is considered here, and it depends strongly on the angle of attack, and less so on depth of the foil. The lift is simplified to be only dependent on the angle of attack, which gives

$$F_u = K_u(\alpha_u + \theta) \quad \text{and} \quad (4.1.9)$$

$$F_f = K_f\theta. \quad (4.1.10)$$

Combining equations 4.1.9 and 4.1.7 above in state-space form gives

$$\begin{bmatrix} \dot{\zeta} \\ \ddot{\zeta} \\ \dot{\theta} \\ \ddot{\theta} \end{bmatrix} = \underbrace{\begin{bmatrix} 0 & 1 & 0 & 0 \\ -\frac{k_{\zeta}}{m} & -\frac{c_{\zeta}}{m} & K_u + K_f & 0 \\ 0 & 0 & 0 & 1 \\ 0 & 0 & -\frac{k_{\theta}}{I} - \frac{L_f K_u}{I} & -\frac{c_{\theta}}{I} \end{bmatrix}}_{\mathbf{A}} \begin{bmatrix} \zeta \\ \dot{\zeta} \\ \theta \\ \dot{\theta} \end{bmatrix} + \underbrace{K_u \begin{bmatrix} 0 \\ \frac{1}{m} \\ 0 \\ -\frac{L_f}{I} \end{bmatrix}}_{\mathbf{B}} \alpha_u \quad (4.1.11)$$

$$\begin{bmatrix} \zeta \\ \theta \end{bmatrix} = \underbrace{\begin{bmatrix} 1 & 0 & 0 & 0 \\ 0 & 0 & 1 & 0 \end{bmatrix}}_{\mathbf{C}} \begin{bmatrix} \zeta \\ \dot{\zeta} \\ \theta \\ \dot{\theta} \end{bmatrix} + \underbrace{\begin{bmatrix} 0 \\ 0 \end{bmatrix}}_{\mathbf{D}} \alpha_u \quad (4.1.12)$$

A, **B**, **C** and **D** of the state-space representation are indicated above.

4.2 Modelling verification and tuning using system identification

As mentioned above, experimental parameter identification was used to obtain the values of the coefficients introduced above and to verify the usefulness of the state-space model presented. Parameter estimation is an often-used technique to determine or refine parameters of a time-invariant system. It has been used extensively with good results in the aircraft industry. Maine & Iliff (1986) gives a thorough overview of the field, with practical methods of implementation of this technique.

The technique involves experimentally stimulating the system with a predefined control and/or disturbance input, and measuring the output states. The input is also sent to the LTI model of the system, which is as representative as possible of the dynamics of the system. The outputs are compared, and an optimization algorithm is used to minimise the difference between the measured and predicted outputs.

A system identification program Milne (2000) for MATLAB was used for the above. It uses the Newton, Levenberg-Marquardt and constrained-Newton optimisation algorithms to estimate the parameters, their Cramer-Rao bounds

(degree of uncertainty) and the experimental measurement noise. Experiments performed were at 4, 5, 6 and 7 m/s, as in the uncontrolled experiments. For full detail of the experimental setup, refer to section 5.3.

The input signal is shown in figure 4.2, and was suggested by Browne (2005) as it is made up of step inputs, theoretically stimulating the full range of input frequencies. These steps also vary in length to ensure that a full range of frequencies are stimulated. A range of amplitudes was used for each speed, to be able to ascertain the effect of control amplitude on the linear range of applicability for the model.

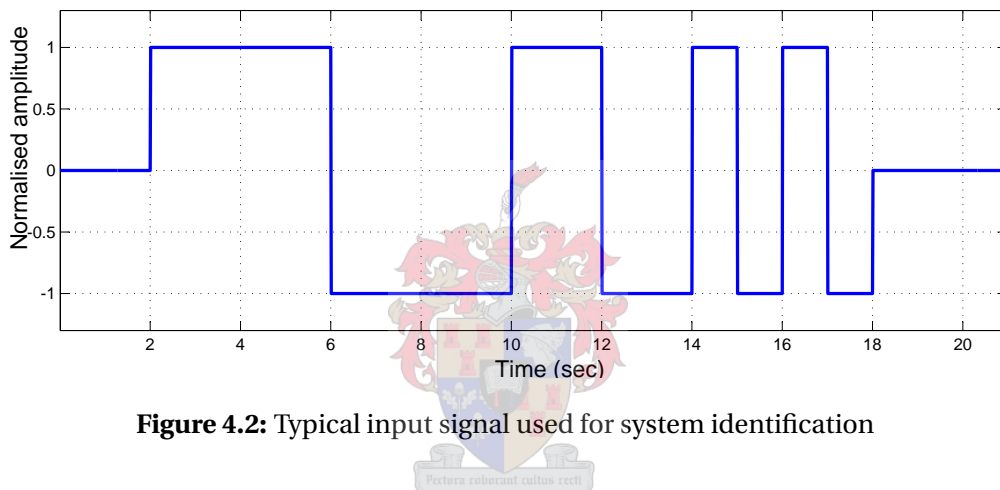


Figure 4.2: Typical input signal used for system identification

4.2.1 System ID inputs and assumptions

Once the linear state-space structure of the model was assumed (section 4.1), the necessary inputs to the parameter estimation program could be determined. These involved all the necessary parameters for the state-space model, initial states for the system as well as optimisation control parameters, and are described below.

For the mass m and moment of inertia I , the values measured in the experiments in appendix A and given in table 5.2 were used. It may seem necessary to increase these values by the added mass and added moment of inertia, but because the model is assumed linear, this is not necessary. The values obtained from the estimation will not be compared to actual 'springs' or

'dampers', which means that the scaling that occurs from this assumption is acceptable. One of the objectives of this project is to have a repeatable design process, also motivating using easy-to-measure parameters such as actual measured mass and inertia of the model.

However, the remaining six parameters still did not have a unique set of values replicating the measured outputs for the input used, i.e. the system is still over-parameterised. It was found that if values were assigned to two additional parameters, the optimisation algorithm used converged to a unique solution. It was decided to model the main and trim foil lift gains to obtain a realistic value, and then to use the parameter estimation for the remaining four parameters, i.e., the pitch and heave stiffness and damping values.

For modelling of the foil lift, the Peter du Cane hydrofoil theory is used as given in appendix B. As is done in airfoils, the two-dimensional theoretical lift curve slope of 2π is modified based on geometry, three-dimensional effects and a loading profile (elliptic). Unique to hydrofoils, free-surface effects are also taken into account depending on the submergence ratio and Froude number for the foil. With this theory, the lift gains for the main and control foils used are $K_f = 400 \text{ N/rad}$ and $K_u = 315 \text{ N/rad}$, respectively. These values do not depend on the foil depth or vessel speed, but it can be shown that these variations, if they are linearised, can be grouped with the other parameters to be estimated, especially the pitch stiffness.

The remaining inputs for the algorithm were determined as follows:

- The starting values for the parameters to be estimated were obtained from inspection of the frequency response measured in section 5.2, as well as the time response of the system and heuristically adjusting the input parameters;
- Because the model used only deals with the system changes around a steady-planing operating point, the initial states of the system were all set to zero. This meant that the cropping of the data to be estimated needed to begin with a steady portion of zero data with no control signal. Thus the measured states and control values were shifted so that

their starting values were at zero before initiating the optimisation algorithm;

- The optimisation control parameters used dictate the maximum number of iterations, the relative change to indicate convergence, and the system's frequency cutoff for estimation of noise in the signals. Respectively, these were set at a maximum of 100 iterations, 0,0001 as the relative change and 4 Hz as the approximate cutoff frequency of the system.

4.2.2 System ID results

The results obtained from the parameter estimation algorithm represented the measured data to varying degrees. An example of a good prediction of the experimental data is shown in figure 4.3. As can be expected, the representation was better at the mid-range amplitudes. At the lower amplitudes, the output was not large enough to be detectable, and at higher amplitudes, nonlinear effects began to come into play. An example of a larger-amplitude result is shown in figure 4.4.

The parameter estimation was performed on four parameters, namely k_z , k_θ , c_z and c_θ . The values estimated for each run are compared in figures 4.5, 4.6, 4.7 and 4.8, respectively, along with their 3σ Cramer-Rao error bounds as estimated by the optimization algorithm. The values are grouped according to speed and ordered by input signal amplitude (increasing from left to right) within each speed group.

From the above estimation of the four parameters, a set of system equations can be set up to represent the system at the speeds investigated. This can be done for each of the speeds and/or expected amplitudes if necessary, but for the purposes of this project, a set of representative values is needed for the control design process. This is because the control algorithm to be used will not be adaptive according to the conditions, but is intended to be generic. As can be seen from the results given, consistent parameter estimation was only achieved for the speeds of 4, 5 and 6 m/s, which is the range of speeds over which the chosen model will apply. The mean values were calculated for the

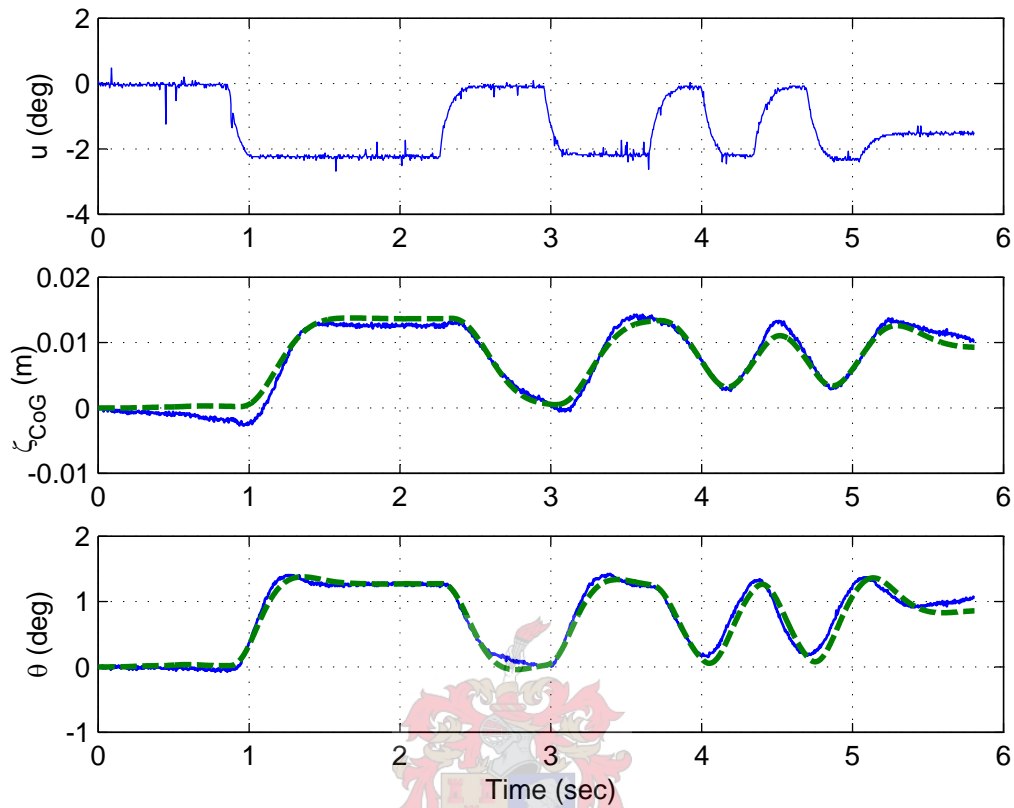


Figure 4.3: Example of good parameter estimation result.

data shown above, and the results for the four parameters are given in table 4.1.

4.2.3 Calculation of model damping and natural frequencies

From the above system of equations, a vibration analysis can be performed to determine the natural frequencies and damping of the system. This is done using the eigenvalues of the system as given by Inman (2001), as well as the representative system coefficients at 5 m/s given above, which is used for the control design.

If a vector is formulated of the eigenvalues of the system matrix \mathbf{A} , in this case

$$\lambda = \lambda_{j,j=1,2,3,4} = \left[-5,85 \quad -148,84 \quad -4,22 + 7,45i \quad -4,22 - 7,45i \right]^T \quad (4.2.1)$$

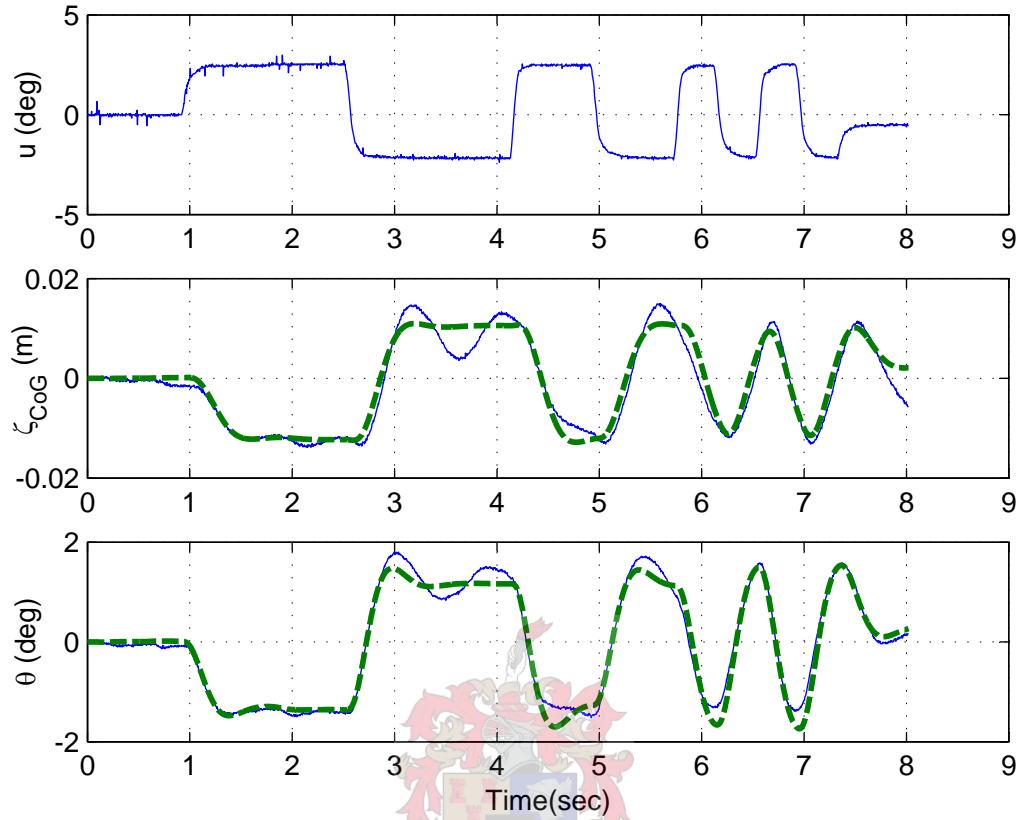


Figure 4.4: Example of a large-input-amplitude parameter estimation result. Note the difference in response in the up- and downwards motions, showing the system nonlinearity for this case.

For each of these eigenvalues, the following are applicable:

$$\omega_{n,j} = \|\lambda_j\| = \sqrt{\Re(\lambda_j)^2 + \Im(\lambda_j)^2} \quad (4.2.2)$$

$$\zeta_j = -\frac{\Re(\lambda_j)}{\omega_{n,j}} \quad (4.2.3)$$

Using the above, the following are obtained:

$$\omega_n = \begin{bmatrix} -5,85 & -148,8 & 8,57 & 8,57 \end{bmatrix}^T \quad \text{and}$$

$$\zeta = \begin{bmatrix} 1 & 1 & 0,493 & 0,493 \end{bmatrix}^T$$

The above results are only applicable for the under-damped case, meaning

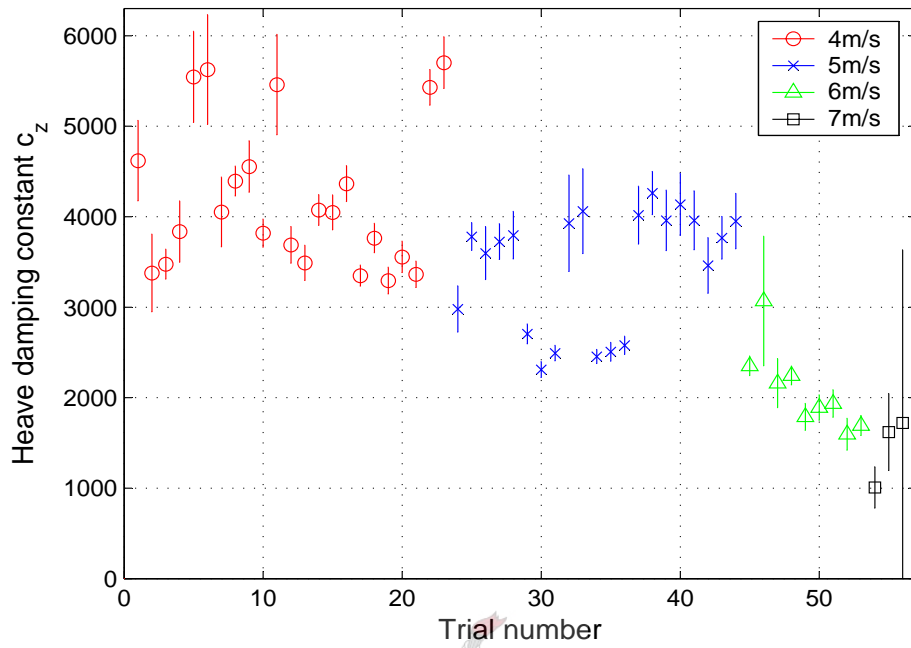


Figure 4.5: Estimated heave damping parameter c_z . Speed groups are sorted by increasing amplitude from left to right.

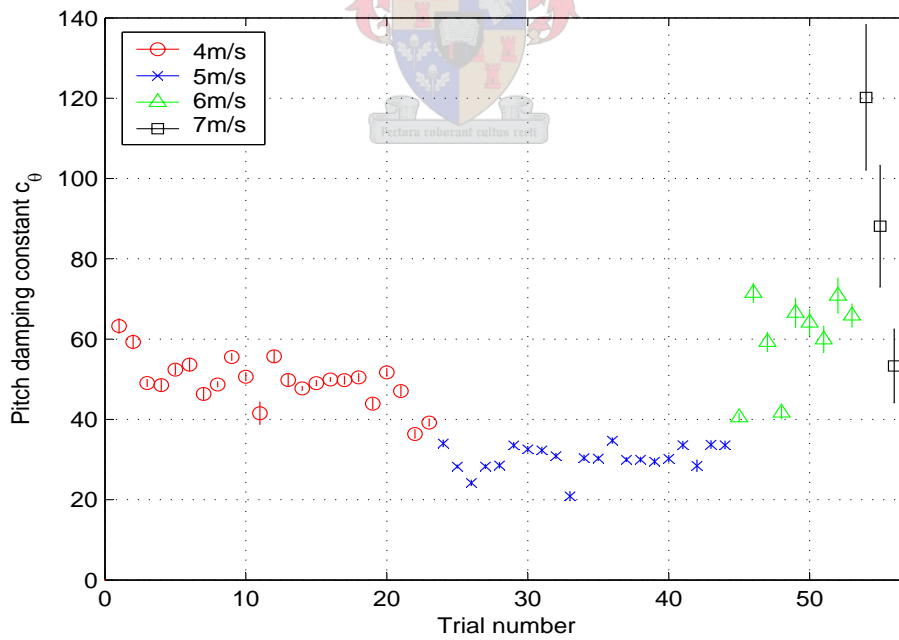


Figure 4.6: Estimated pitch damping parameter c_θ . Speed groups are sorted by increasing amplitude from left to right.

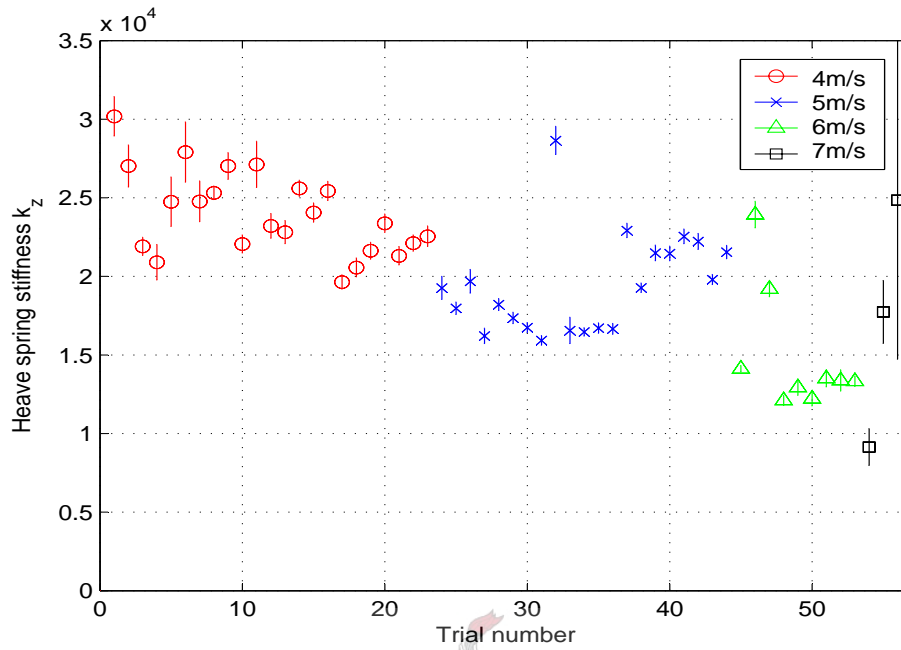


Figure 4.7: Estimated heave spring stiffness parameter k_z . Speed groups are sorted by increasing amplitude from left to right.

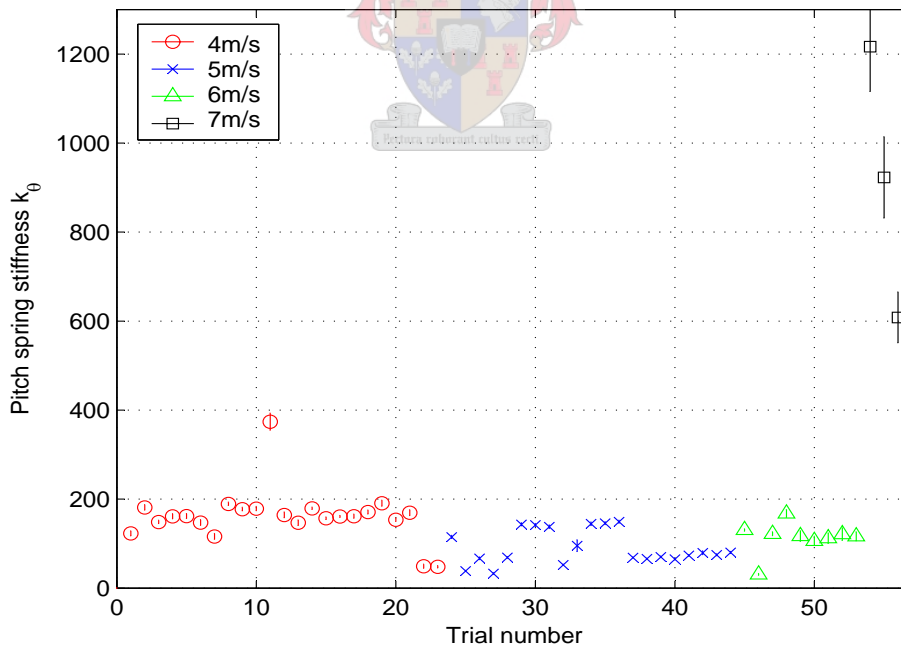


Figure 4.8: Estimated pitch spring stiffness parameter k_θ . Speed groups are sorted by increasing amplitude from left to right.

Table 4.1: Parameter values estimated from system identification results

Parameter	k_ζ (N/m)	k_θ (N/rad)	c_ζ (N·s/m)	c_θ (N·s/rad)
4 m/s	$2,40 \times 10^4$	161	$4,21 \times 10^3$	49,6
5 m/s	$1,94 \times 10^4$	91	$3,45 \times 10^3$	30,4
6 m/s	$1,50 \times 10^4$	114	$2,08 \times 10^3$	60,0
7 m/s	$1,72 \times 10^4$	916	$1,45 \times 10^3$	87,2

that only the 3rd and 4th identical values refer to the natural frequency and damping of the system. Thus, at this speed the natural frequency and damping are as follows:

$$\omega_n = 8,57 \text{ rad/s}, \therefore \omega_n \sqrt{L/g} = 3,14 \quad (4.2.4)$$

$$\zeta = 0,49 \quad (4.2.5)$$

From this, the measured damped natural frequency should be $\omega_d = \omega_n \sqrt{1 - \zeta^2} = 7,45 \text{ rad/s}$, $\therefore \omega_d \sqrt{L/g} = 2,73$, approximately the value seen in the peak of the measured response at 5 m/s in section 3.4. Using the above method, the natural frequency, damping ratio and damped natural frequency is given in table 4.2 below for the full range of speeds. It can be seen how the results at 7 m/s do not represent the natural frequency measured in the previous chapter.

Table 4.2: Vibration analysis results

	ω_n (rad/s)	ζ	ω_d (rad/s)
4 m/s	9,63	0,71	6,74
5 m/s	8,57	0,49	7,45
6 m/s	8,93	0,93	3,22
7 m/s	17,39	0,70	12,5

Chapter 5

Experimental validation

In the previous chapters, results are presented for hydrodynamic modelling and state-space modelling experiments. In this chapter, a description is given of the setup and methods that were used for these, as well as the control experimentation in the next chapter. As far as possible this experimentation was done according to the International Towing Tank Convention (ITTC) guidelines, *ITTC - Recommended Procedures, High Speed Marine Vehicles, 7.5-02-05*.

The experimental facilities common to all tests performed are first described in section 5.1. After this, the two particular experimental setups that were used are described in more detail. They are:

1. The original model was tested with the two trim foils at the stern using a LABVIEW data acquisition program. Details are given in section 5.2;
2. The model was modified to have a single trim foil at the stern, this time with an adjustable angle-of-attack controlled by a servo motor. This was used for the state-space modelling and control phases of the project. The data acquisition and control was done using a MATLAB-based real-time toolbox. Details are given in section 5.3.

Section 5.4.2 concludes this chapter with an analysis of errors to be expected from the experimental setup that was used, as well as tests to ensure that it performs as expected. These include tests for the backlash, time delay and speed of the system.

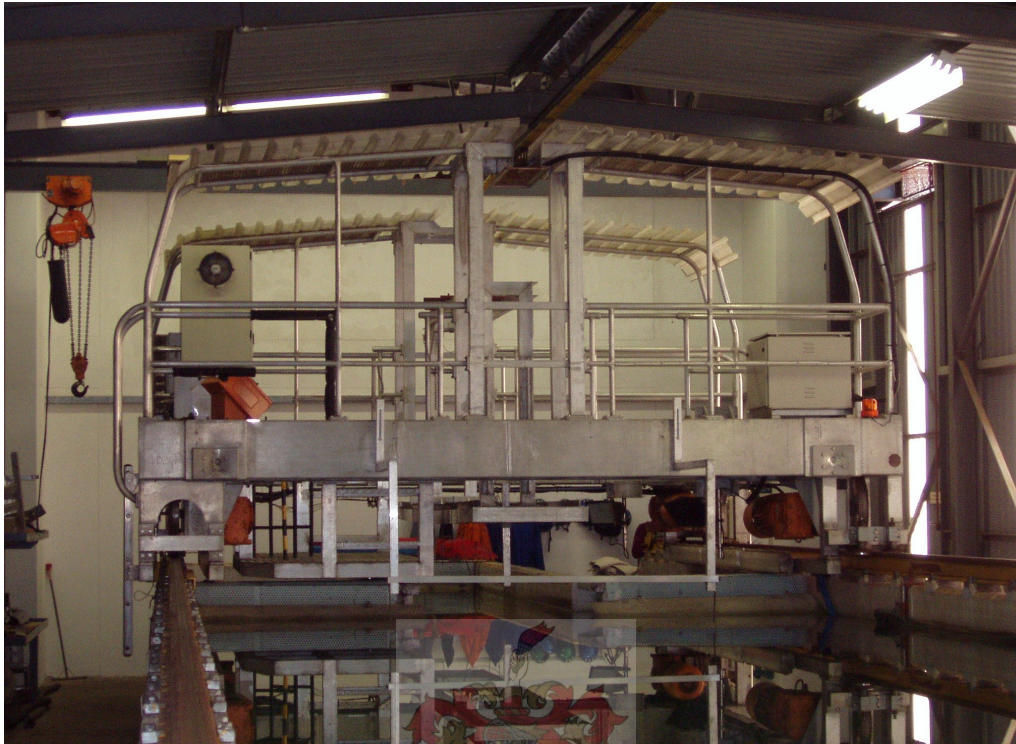


Figure 5.1: The towing tank, along with the trolley used in testing

Table 5.1: Sensor specifications and values measured

Value sensed	Variable	Units	Sensor specifications
Model velocity	V	m/s	Trolley mounted tachometer
Model resistance	T	N	50 kg load Cell
Bow height	h_b	m	Potentiometer coil displacement sensor
Stern height	h_s	m	"
Wave height	h_{wave}	m	Senix®TS-30S ultrasonic distance sensor

5.1 Experimental facilities used

The experimental setup was located in the Department of Mechanical Engineering's 90 m long towing tank. This tank is 4,63 m wide and 2,3 m deep, and is equipped with a self-propelled trolley which can be driven up to 9,5 m/s. This provides adequate speed range to test the model in planing Froude numbers. A photograph of the trolley is provided in figure 5.1.

On the trolley, experimental data can be obtained from 5 sensors. They

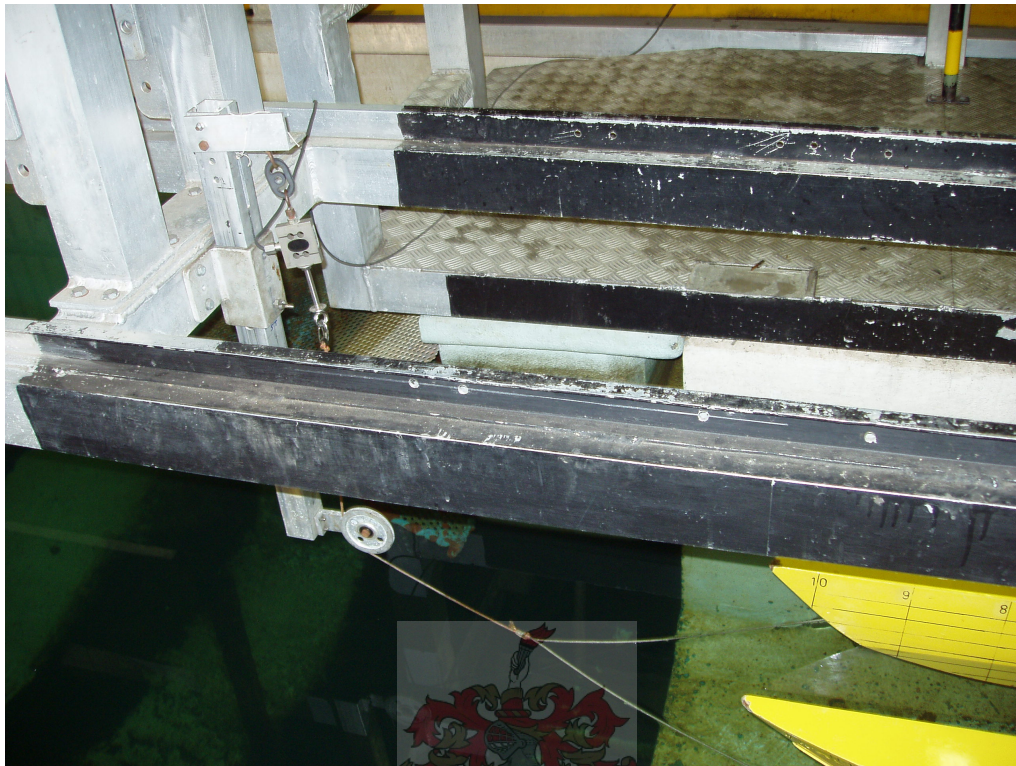


Figure 5.2: The load cell used in determining the vessel drag, along with the sling arrangement for towing

are listed in table 5.1. The sensors are part of a data acquisition (DAQ) system which feeds all the signals to a signal conditioning box which provides 0-10 V analogue outputs. The load cell is shown in figure 5.2 along with the sling arrangement for towing the vessels. One of the trim sensors is shown in figure 5.3.

Calibration was only needed for the trim sensors, as the other sensors (speed and load) have been precalibrated. The wave height sensor was used at its factory calibration. An error analysis for the values calculated from the sensors is given in section 5.4.2.

To obtain the gain of the trim sensors, the output voltage was measured at zero and 0,3 m extensions. For the zero offsets, trim and water height measurements were taken for the vessel at rest in still water. The water height was also measured for the full length of the tank without the model to check that



Figure 5.3: Trim sensor used to measure displacement of the model's bow and stern

the trolley tracks are indeed parallel to the water surface. The results obtained were within the sensor accuracy range, so a smooth and level track surface was assumed.

5.1.1 Details of HYSUCAT model

The model boat used is shown in figure 5.4. It is a HYSUCAT model with flat vertical hulls on the tunnel side of the demihulls. The specifications of the model are provided in table 5.2. The experimental determination of these parameters is described in appendix A.

The model was towed using hitch points near the centre of gravity, allowing pitch, heave and roll motions with minimal interference. The towing angle used was 5° above horizontal, and this value was also used in the POWERSEA simulations described in chapter 3.

The hydrofoils used on the model were according to the typical HYSU-

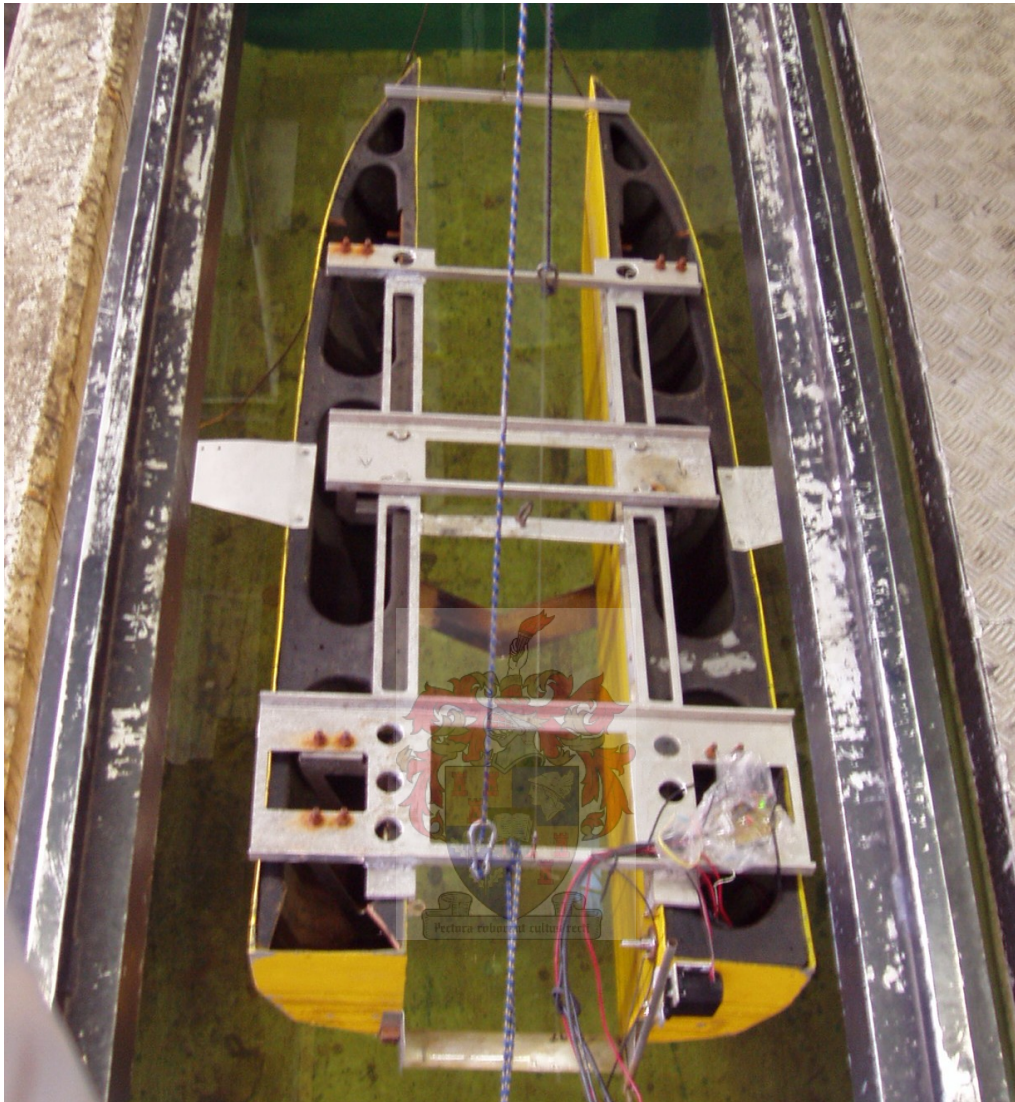


Figure 5.4: Model HYSUCAT used in this study

Table 5.2: Measured model HYSUCAT parameters

Parameter	Value
Scaling factor λ	8:1
Mass of model	22,29 kg
Vertical centre of gravity (from baseline)	0,16 m
Horizontal centre of gravity (from stern)	0,548 m
Pitching radius of gyration r_G	0,402 m
Static trim (bow up pos)	0,2°

CAT configuration, with a main foil near the centre of gravity supporting the weight of the vessel, and trim foils at the stern to adjust the vessel trim and increase stability. Further details of the measurements taken from them for the POWERSEA inputs are given in table 3.2 in section 3.2.

5.1.2 Wave generation

Wave generation for the experimentation is achieved by a wave generator at the far end of the tank, so that the tests can only be carried out in head seas. The wave generator is of the pneumatic type, which produces cyclical air pressure on the water surface by a rotating choke valve. It is shown in figure 5.5, where the fan ducting can clearly be seen.

The wave frequency is practically variable between about 1,5 and 5,5 rad/s. At lower frequencies, wave absorbers on the sides and end of the tank are not fully effective, and reflected waves add unacceptable noise to the waves produced. At higher frequencies, the wave damping over the length of the tank are such that waves at the start of the run are too small for useful measurements. The wave frequency can only be set approximately, which means all wave frequencies reported in this project are those measured by the wave height sensor - this makes them significantly more accurate.

The amplitude of the waves produced can be varied by switching on one or both of the fans which produce the air pressure. Only the full wave height was used in this project, as investigation into the linearity of results requires several wave heights, and the measured variation of the wave rms produced by the single fan is only 7% less than that from both fans. The variation of wave amplitude with wave frequency is shown below in figure 5.6. It can be seen that wave heights in the mid-frequency range are higher than those at low or high frequencies, as can be expected.

5.2 Validation of POWERSEA simulations

For the validation of the model's motions using POWERSEA, a simple data acquisition system was used. The voltages read from the sensors were digitized



Figure 5.5: The towing tank wave generator

using an Eagle Technologies USB-26 μ DAQ card. The data was then logged using LabVIEW 7.1 via a USB 1.1 port. This setup was only used for this set of experimental runs, and a more advanced real-time setup was used for the controlled runs (see section 5.3 for details).

5.2.1 Experimental scope

The experiments performed measured the model response to variation of the model velocity and wave frequency. Variation of the wave height was not possible, as the wave generator installed is limited to one wave height. The velocities used were 4, 5, 6 and 7 m/s, which is equivalent to $F_{nV} = 2,41 - 4,2$. Wave frequencies used were (0,3 0,4 0,5 0,6 0,7 0,8)Hz, which is the usable range available from the wave generator. The frequency cannot be set exactly, so the values above are only approximate. The actual frequencies of the waves generated were obtained from the postprocessing of the wave height data from

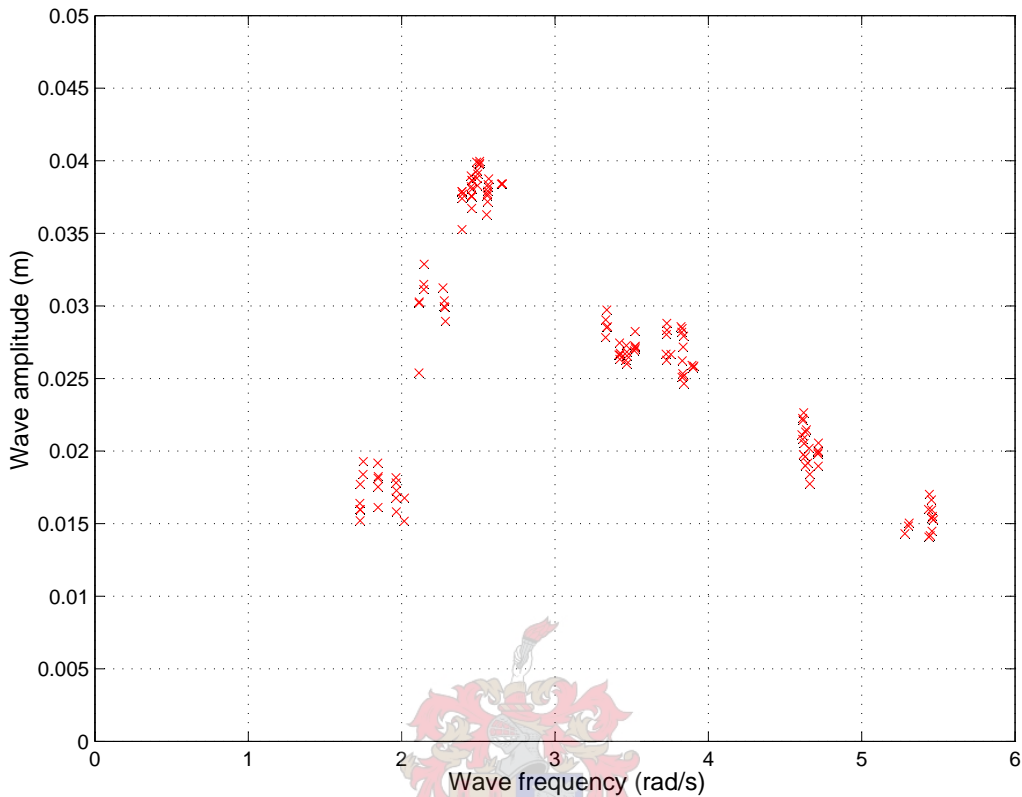


Figure 5.6: Measured wave amplitude vs wave generation frequency

the wave height sensor.

5.2.2 Postprocessing of results

The postprocessing of the data obtained was done using the following steps:

1. The velocity profile of the towing tank run was plotted. From this, the constant speed section of the data was cut, using graphical determination of the start and end times;
2. The DAQ card occasionally gave voltage 'spikes'. These were filtered out, as they happen at a frequency that is much higher than any physical frequency observable;
3. The constant velocity for the run was obtained by using the mean of the velocity cut in 1. above;

4. As the wave height sensor is located 1,626 m in front of the centre of gravity of the model, the wave data measured was not that experienced by the model. The measured data were shifted in time to those wave heights experienced by the centre of gravity using

$$t_d = L_{waveht-CG}/V. \quad (5.2.1)$$

The centre of gravity will experience the wave t_d seconds later than the wave height sensor;

5. The measured voltages were converted to their appropriate values using the calibration gains and zero offsets. The heave and pitch of the model were calculated from these using

$$\zeta_{CG} = \left(\frac{\zeta_b L_s}{L_b + L_s} \right) + \left(\frac{\zeta_s L_b}{L_b + L_s} \right) - \zeta_0 \quad \text{and} \quad (5.2.2)$$

$$\theta = \arcsin \left(\frac{\zeta_b - \zeta_s}{L_b + L_s} \right) \quad (5.2.3)$$

where $L_b + L_s$ is the sum of the bow and stern trim-sensor-to-centre-of-gravity lengths.

6. A power spectral density (PSD) calculation was done on the heave, pitch and wave height data. The PSD was an FFT of the data using a single Hanning window of the whole data, with no overlap and a 95% confidence interval. The data displayed in the frequency domain allowed inspection of how close the motions and waves were to a pure sinusoid, and determination of the frequency and amplitude of the primary signal, the maximum in the Fourier series.
7. The heave Response Amplitude Operator (RAO) was calculated from the ratio of the amplitude of the heave rms to that of the wave input. This RAO value was plotted against $\omega_e \sqrt{L/g}$, the normalised encounter frequency. The results of this are given in comparison to POWERSEA simulations in section 3.4.

8. The pitch RAO uses the pitch rms response over the time measured, divided by the wave rms and the wave number. The results of this are also plotted against $\omega_e \sqrt{L/g}$ in section 3.4.

5.3 System identification and control system validation

The above experimental setup was modified from a passive to an active system for the system identification and control system testing stages of the project. The aim was to have a dynamically similar system, but with controllable trim foils at the stern. This section describes the system hardware and software design process.

5.3.1 Control hardware and software

There are many configurations of control surface(s) for controlling pitch and heave of a vessel. Investigation of this is outside the scope of this project, however, and certain assumptions were made as to the design of the control surface. Among these were the location of the foil, which was at the stern of the vessel.

For hardware to adjust the angle of attack of the trim foil(s) at the stern, the aim was to have a very simple and functional mechanism to achieve this. Thus it was decided to use a single trim foil spanning the tunnel, and to mount the mechanism on the stern instead of integrating it into the vessel. This made it easy to adjust as necessary. The final design of the mechanism is shown in figure 5.7, and drawings are given in appendix C.

Because the mechanism is situated behind the stern of the vessel, the ends of the foil were seen to be susceptible to ventilation from the vessel's dry transom. This effect did not always occur, but was not easily predictable and/or reproducible. The foil was thus separated from the ventilated area to prevent this ventilation from happening by means of 'fences'. One of these can clearly be seen in figure 5.7, situated at the lower stern of the vessel. These fences

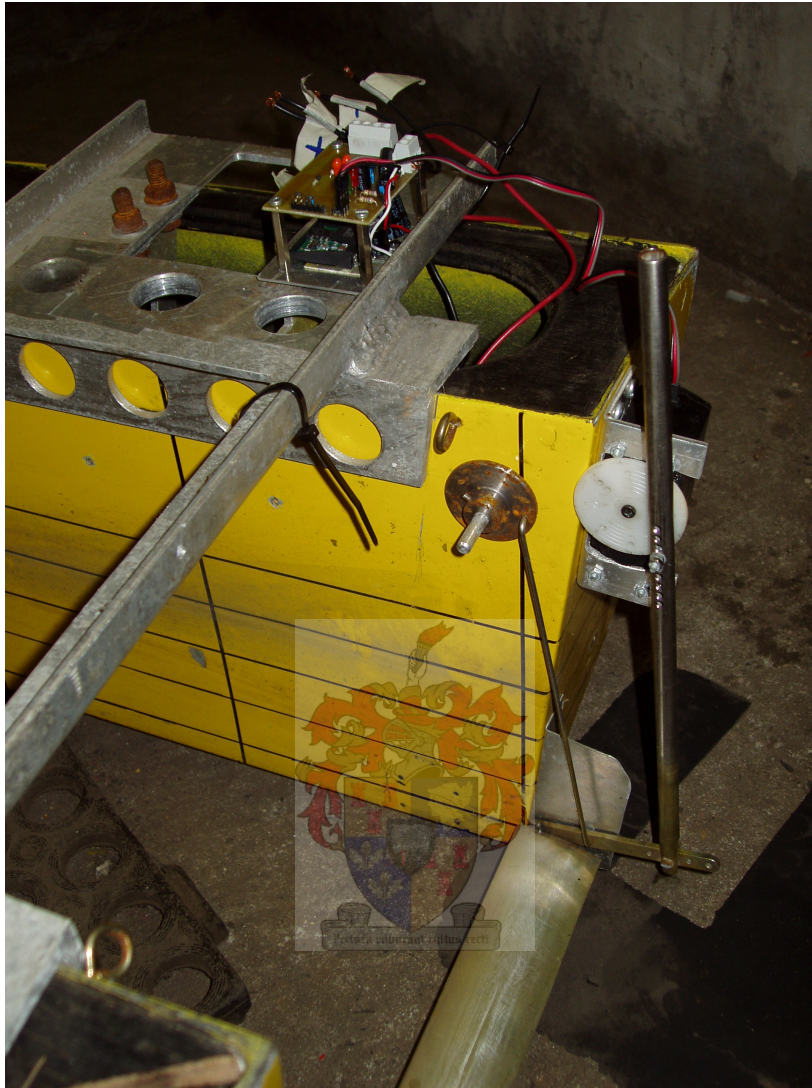


Figure 5.7: The trim foil control mechanism at the stern of the model

were effective in preventing ventilation, as the problem was not encountered after they were installed.

The servo attached to the foil control mechanism can also be seen in figure 5.7. The specifications of the servo are given in table 5.3. Sizing of the servo was difficult, in part due to the uncertainty of time-dependant forces on the trim foil. Also, the torque needed from the servo is dependant on the centre of lift of the foil, which varies with angle of attack Houghton & Carpen-

Table 5.3: Servo specifications

Parameter	Value
Make and model #	Eagle (JR) 615-Jumbo servo
Torque rating	18 kg · cm
Speed rating	0,2 s/60°
Angle range	approx. 90°
Approx size + weight	±80 × 60 × 40 mm, ±0,1 kg

ter (1993). The value typically used for design purposes is approximately $c/4$ from the leading edge, where c is the chord length of the foil. This motivated the positioning of the foil hinges slightly in front of $c/4$ for foil stability in the case of insufficient control forces.

The servo is controlled using a DC-to-PWM servo driver, which was custom-made by students of the Electronic Systems Laboratory (ESL) at the Department of E&E Engineering (SU). A circuit diagram for the driver and basic usage instructions are given in appendix D.

Communication between the above servo driver and the laptop computer was achieved by a National Instruments PCMCIA card (NI DAQcard 6024-E). This card was used because it is significantly faster than the USB card used in the uncontrolled experiments (see section 5.2), and has 2 analogue outputs for controlling the trim foil. Also, it is well-supported by both the LABVIEW and Humusoft real-time software packages available.

The Humusoft real-time toolbox for MATLAB is designed as an interface between MATLAB and/or SIMULINK, and provides good access to the Windows kernel for reading and writing values to DAQ hardware. It has driver support for the DAQcard 6024E used, which means that it was quite easy to use, with minimal programming necessary.

A schematic of the above experimental system layout is given in figure 5.8, where the physical hardware and digital components can be seen, as well as the analogue electrical connections between them.

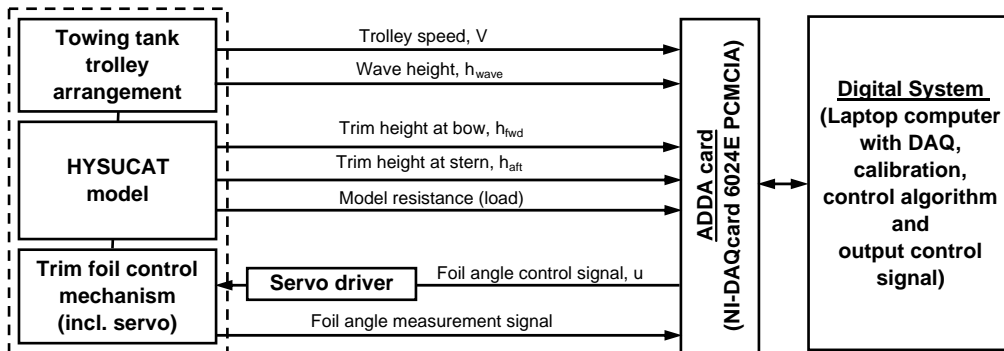


Figure 5.8: Schematic layout of experimental system

5.3.2 Parameter estimation and control system implementation

The parameter estimation and control experimentation involved the hardware shown schematically in figure 5.8, coupled to the digital control strategy implemented in SIMULINK. The Humusoft real-time toolbox provided the interface between the two. The highest speed available from single-read, single-ended measurements across all the channels varied somewhat, necessitating a sample rate at which the system would always work. The system sometimes worked with a sample rate of up to 1000 Hz, but was unpredictable. Thus a sample rate of 250 Hz was settled on, which provided near 100% execution of the algorithms.

5.4 Experimental setup testing and error analysis

To ascertain the accuracy and reliability of the results received from the system, several tests were carried out. The accuracy to be expected from the sensors was also considered, as this also gives an indication of the fidelity of the results presented.

5.4.1 System performance testing

Due to the fact that the system speed was a limiting factor to the performance of the physical control system, several checks were run to identify possible problem areas as well as suggest improvements which can be made.

Servo slew rate An important performance factor is the servo 'slew rate', which is the angular velocity that is attainable. This was tested with the control mechanism and potentiometer attached, and the manufacturer's claim of $0,2 \text{ s}/60^\circ$ was reached, showing that the servo is powerful enough to drive the whole mechanism. To improve the speed of the foil, either a quicker servo could be bought, or the system could be geared up, as it does seem powerful enough for the task. Faster servos were considered, but there were limited options in the RC hobby range, and at much higher cost (approx $3\times$) for nominal increases in speed. Gearing up the system is an option, however, and the system was sped up by 16% with the current arrangement. Further gearing was attempted, but it caused problems with backlash, as well as reaching the limiting stops of the servo - a servo was actually burnt out by this. There is definitely scope for improvement, but it needs to be done with care.

Backlash The backlash of the system was tested by fixing the servo position while moving the mechanism to its limits. A maximum of 1° was measured in the foil angle near the extremes, with typical values of about $0,5^\circ$. This depends primarily on the bolted joints used in the foil linkage, as the servo itself has very little backlash.

Maximum foil angle The foil angle available with the linkage is $-16,0^\circ$ to $18,5^\circ$ relative to the vessel baseline. From foil theory, this is sufficient range to cover up to the stall point in the up- and downwards positions.

Ventilation of control foil Ventilation of the control foil was observed, drastically reducing the foil lift and thus the control authority. Ventilation screens, or 'fences' were installed, ameliorating the situation considerably.

5.4.2 Error analysis

An error analysis was performed to determine the maximum bias error of the outputs at a representative measured point. The approach followed is the ISO method of error estimation and is given by Granger (1998). If a function $F = f(X_1, X_2, X_3 \dots)$, where F is the calculated output and X_j are the measured inputs, then the bias error B_F is given by

$$B_F^2 = \left(\frac{\partial F}{\partial X_1} B_{X_1} \right)^2 + \left(\frac{\partial F}{\partial X_2} B_{X_2} \right)^2 + \dots \quad (5.4.1)$$

For the heave calculation using equation 5.2.2, the following can be derived using ζ_b and ζ_s as X_1 and X_2 :

$$B_{\zeta_{CG}}^2 = \left(\frac{L_s}{L_s + L_b} B_{\zeta_b} \right)^2 + \left(\frac{L_b}{L_s + L_b} B_{\zeta_s} \right)^2 \quad (5.4.2)$$

Thus, using $L_b = 0,767$ m and $L_s = 0,548$ m, as well as assuming $B_{\zeta_b} = B_{\zeta_s} = 1,5 \times 10^{-3}$ m, we obtain a heave bias error of $B_{\zeta_{CG}} = 8,8 \times 10^{-4}$ m, or approximately 2,95% of the nominal measured value.

Similarly, for pitch we have, after taking partial derivatives of θ (see 5.2.3) w.r.t. ζ_b and ζ_s :

$$B_{\theta}^2 = \left(\frac{1}{\sqrt{(L_b + L_s)^2 - (\zeta_b - \zeta_s)^2}} B_{\zeta_b} \right)^2 + \left(\frac{-1}{\sqrt{(L_b + L_s)^2 - (\zeta_b - \zeta_s)^2}} B_{\zeta_s} \right)^2 \quad (5.4.3)$$

Using the small angle approximation that $\zeta_b - \zeta_s \ll L_b + L_s$ and the bias errors above, this simplifies to $B_{\theta} = \frac{\sqrt{2}}{L_b + L_s} B_{\zeta_b}$ which, with the same substitutions as those above, give us $B_{\theta} = 1,14 \times 10^{-3}$ rad, meaning that the percentage bias error is approximately 3,8%.

For the wave height sensor, the error quoted is $0,8 \times 10^{-3}$ m, which gives it a percentage bias error of about 2,6%. All the above errors indicate that the error level, while noticeable, is not large enough to cause significant uncertainty in the results presented.

Chapter 6

Control system design and implementation

Chapters 3 and 4 dealt with the modelling and identification of the dynamics of a HYSUCAT in waves and in smooth water, respectively. Once a reasonable state-space model of the system was obtained, the control design could be carried out.

6.1 Model summary for control application

To obtain a single controller design usable over the whole speed range of interest, a design point was chosen. Due to the problems encountered at 7 m/s caused by the sensitivity and speed of the vessel response, as well as the short test time (≈ 6 s), the control design and testing was carried out for 4, 5, and 6 m/s speeds. The control design point was thus set at 5 m/s.

From the system identification results provided in section 4.2.2, the estimated parameters at this design point are used. For the first control design iteration, representative parameter values were first roughly estimated from the system identification results. For the revised controller design given in section 6.2.3, these were refined specifically for the design point. At the de-

sign point, the equations are:

$$\begin{bmatrix} \dot{\zeta} \\ \ddot{\zeta} \\ \dot{\theta} \\ \ddot{\theta} \end{bmatrix} = \underbrace{\begin{bmatrix} 0 & 1 & 0 & 0 \\ -870 & -155 & 32,1 & 0 \\ 0 & 0 & 0 & 1 \\ 0 & 0 & -73,4 & -8,4 \end{bmatrix}}_{\mathbf{A}} \begin{bmatrix} \zeta \\ \dot{\zeta} \\ \theta \\ \dot{\theta} \end{bmatrix} + \underbrace{\begin{bmatrix} 0 \\ 14,13 \\ 0 \\ -48,1 \end{bmatrix}}_{\mathbf{B}} \alpha_u \quad (6.1.1)$$

$$\begin{bmatrix} \zeta \\ \theta \end{bmatrix} = \underbrace{\begin{bmatrix} 1 & 0 & 0 & 0 \\ 0 & 0 & 1 & 0 \end{bmatrix}}_{\mathbf{C}} \begin{bmatrix} \zeta \\ \dot{\zeta} \\ \theta \\ \dot{\theta} \end{bmatrix} + \underbrace{\begin{bmatrix} 0 \\ 0 \end{bmatrix}}_{\mathbf{D}} \alpha_u \quad (6.1.2)$$

6.1.1 Control system modelling

To test the control systems that will be designed, a time simulation of the system was implemented. Modelling of the system itself, as well as the effect of the control surface is covered by the equations presented in section 4.1. For the forces on the vessel from waves, the potential-flow method attempted in section 3.4 was not detailed enough. As the control system is to be designed at a design point, representative wave disturbance forces were thus used, and the control results optimised at that point.

For the wave disturbance forces experienced by the vessel, only the resultant wave forces were considered, divided into a heave disturbance force in the vertical direction at the centre of gravity, as well as the pitch moment at this point. To obtain these force values, Newton's second law was applied, with the vessel accelerations from one of the preliminary tests at the design point as inputs. These are given by:

$$\vec{F} = m\vec{\zeta} \quad \text{and} \quad \vec{M} = I\vec{\theta} \quad (6.1.3)$$

This input set represents the forces experienced by the model vessel at the design point, based on the overall motions measured. With the system model completed, the control design can now be carried out.

6.2 Controller types and strategies

To design of a controller for this system, many options are available. Strategies involve both the linear and nonlinear controller types, control of one or both output states. Also, a 'predictive' controller can be implemented by the use of disturbance estimation or other forward-looking techniques.

To start with, a Linear Quadratic Regulator (LQR) was used based on the heave and pitch of the vessel, as well as a nonlinear 'bang-bang' controller. As an attempted improvement on these, the LQR design was revised and based on the forward and aft displacements and velocities. The following sections detail their design.

6.2.1 Pitch and heave output-weighted LQR design

One of the most-used controllers is the linear PID type. The control strategy for a MIMO system is given by

$$\mathbf{u}(t) = \mathbf{K}_P \mathbf{x}(t) + \mathbf{K}_I \int_{t_0}^t \mathbf{x}(t) + \mathbf{K}_D \dot{\mathbf{x}}(t) \quad (6.2.1)$$

where \mathbf{K}_P , \mathbf{K}_I and \mathbf{K}_D are the proportional, integral and derivative constant vectors, respectively, and \mathbf{x} is the state vector. In this application, a proportional full-state feedback controller was designed and tested in this 2-input, 1-output MIMO system. The following gives the motivation for this choice and the controller design process.

Proportional control is the simplest and most-used element of the PID controller. The Linear Quadratic Regulator (LQR) is a method of generating the proportional gains. More details on this are given below.

Integral control was not used, as it tends to give a slower controller, something which is to be avoided in this case. Its primary advantage is to give better steady state tracking, but this is not the primary objective of the controller; rather, the objective is to give good disturbance rejection.

In the case of *derivative control*, the presence of the pitch and heave derivatives in the state vector already provides it to some degree. The second deriva-

tive was not used, despite it being one of the outputs to be minimised, primarily because

- a) the numerical 2nd derivative of a signal with noise tends to contain a low signal-to-noise ratio, and strong filtering in real-time introduces unavoidable time delays in the system and
- b) derivative control is usually only added when optimising a PID controller, and not designed in from the start. This is because derivative control is usually detrimental to the stability of the system.

For the full state feedback design, the states need to be estimated from the outputs, assuming that the system is observable. In this case this is trivial, as the full state vector is simply the two outputs of heave and pitch and their derivatives. Thus Euler numerical derivatives of the outputs were filtered and used to recreate the state vector.

For the full state feedback gains \mathbf{K} , the output-weighted LQR design was used, as given by Franklin *et al.* (1998) and the MATLAB help file documentation (The MathWorks, 2003). It involves determination of the feedback gains \mathbf{K} from the solution of the steady state, or 'algebraic', Riccati equation.

As inputs for this calculation, a weighting matrix is needed for both the individual outputs (\mathbf{Q}) and the control signal u (\mathbf{R}). To determine these, first the weighting between the two outputs was chosen. After this, the control system was gradually given more authority by reducing \mathbf{R} , thus giving the control signal more scope for the foil angle. Naturally, this is limited by the practical operating range of the control surface, which is approximately $\alpha = \pm 15^\circ$.

As the control system has much greater authority over pitch than heave, it would seem that the output pitch weighting should be considerably greater than that for heave. This ($\mathbf{Q} = \begin{bmatrix} 2 & 0 \\ 0 & 8 \end{bmatrix}$) worked well for low control signals, but once the controller started having a significant effect on the pitch, it tended to overreact, and introduce high frequency motions. It was found that a more equal weighting between the two ($\mathbf{Q} = \begin{bmatrix} 5 & 0 \\ 0 & 5 \end{bmatrix}$) improved the response; the heave signal tended to be smoother and thus smooth the control signal without reducing it. If the heave weighting was greater for the pitch ($\mathbf{Q} = \begin{bmatrix} 8 & 0 \\ 0 & 2 \end{bmatrix}$), the con-

trol tended to be more sluggish because the heave motion usually happens after a pitch motion.

Thus equal weighting was used between the pitch and heave. As noted above, the weighting on the control signal was gradually lowered until the control signal was limited by its speed of response or its no-stall operating range. The weighting matrices that were used for this controller were:

$$\mathbf{Q} = \begin{bmatrix} 5 & 0 \\ 0 & 5 \end{bmatrix} \quad \text{and} \quad \mathbf{R} = [0,02] \quad (6.2.2)$$

yielding the following full state feedback controller:

$$u = -\mathbf{K}\mathbf{x} \quad \text{with} \quad \mathbf{K} = \begin{bmatrix} 0,123 & 0,000398 & -13,95 & -0,522 \end{bmatrix} \quad (6.2.3)$$

6.2.2 Bang-bang controller design

As the vessel model used is linear, design of a nonlinear bang-bang controller is somewhat heuristic, and relies on time simulations for its results. Also, experimental tests are needed, as the vessel's response becomes more nonlinear with these sudden changes in input.

Because the motions of the vessel without control are cyclical and oscillate about a point, the bang-bang controller could simply switch between its positive and negative values at a certain state value/combination of values. In non-linear control terms, the pitch and heave oscillations form ellipses on the phase plane diagram (' x to \dot{x} ' plot), and the switching line is centered at the origin and has a defined slope.

For simplicity, this 'switching line' (or switching phase) can be based on the vessel heave, pitch or wave height signals. The *wave height* would be the most stable input as it is not affected by the control system. However, because the wave height would not be directly available to a vessel on the open water without complex instrumentation, it was not used. The vessel's *pitch* is most affected by the control signal, meaning that this can easily cause chattering if the control is effective and/or the motions are small. Thus the *heave* was chosen, as it is less affected by the control system, is more in phase with the

wave signals and is easily measurable.

To actually determine the switching phase, the switching line was calculated such that switching occurred when needed, i.e. the control counteracted the vessel's pitching motions. This was tested experimentally, and from this, the phase was moved earlier and later in time until the system became unstable. Selection of the 'best' controller was based on the amplitude of the motions, as well as the 'apparent stability' of the vessel.

For the switching amplitude, this was varied according to the speed to obtain a control signal that did not overcorrect the vessel's motions. For 4, 5, and 6 m/s speeds, the input step amplitudes were $\pm 2^\circ$, $\pm 3^\circ$ and $\pm 5^\circ$, respectively.

6.2.3 Revised LQR controller based on fore and aft vertical motions and velocities

For the pitch- and heave-weighted LQR, there is no physical link between the pitch values in radians and the heave values in meters. Thus, an alternative LQR design was tested, where the two variables minimised are the forward and aft vertical displacements, both in meters. This was also then repeated using the bow and stern vertical velocities, to investigate whether this provided any significant improvement in the results.

The calculation of the full-state-feedback gains \mathbf{K} for these two methods follows the same approach as that given in section 6.2.1, using the output-weighted solution of the steady-state Ricatti Equation. As mentioned above, the first uses the bow and stern vertical displacements, respectively ζ_b and ζ_s , as the two outputs. They can be written in terms of the pitch and heave, using small angle approximations by

$$\zeta_b = \zeta + L_b\theta \quad \text{and} \quad \zeta_s = \zeta - L_s\theta \quad (6.2.4)$$

where L_b and L_s are, respectively, the lengths between the forward and aft points and the centre of gravity.

Thus the output matrix \mathbf{C} is modified to be

$$\mathbf{C} = \begin{bmatrix} 1 & L_b \\ 1 & -L_s \end{bmatrix} \begin{bmatrix} 1 & 0 & 0 & 0 \\ 0 & 0 & 1 & 0 \end{bmatrix} \quad (6.2.5)$$

Using this, the new outputs were equally weighted for the LQR design ($\mathbf{Q} = \begin{bmatrix} 5 & 0 \\ 0 & 5 \end{bmatrix}$). The weighting of the control signal (\mathbf{R}) was again adjusted by testing until an acceptable control signal was obtained for typical vessel motions. $\mathbf{R} = [0,013]$ was used. The full state feedback gains used are thus

$$\mathbf{K} = \begin{bmatrix} -3,39 & -0,022 & -17,0 & -0,678 \end{bmatrix} \quad (6.2.6)$$

Alternatively, using the forward and aft velocities as the outputs, the matrices \mathbf{C} and \mathbf{K} are

$$\mathbf{C} = \begin{bmatrix} 1 & L_b \\ 1 & -L_s \end{bmatrix} \begin{bmatrix} 0 & 1 & 0 & 0 \\ 0 & 0 & 0 & 1 \end{bmatrix} \quad (6.2.7)$$

$$\mathbf{K} = \begin{bmatrix} 0,84 & 0,022 & -0,0097 & -0,69 \end{bmatrix} \quad (6.2.8)$$

The above gains were used to test these two alternative LQR designs, and they are compared to the original three controllers in the second half of section 6.3 below.

6.3 Control implementation results

The above control strategies were tested using the facilities described in chapter 5. The system was tested for the full range of encounter frequencies at 4, 5, and 6 m/s using fixed foils (no control), the heave- and pitch-weighted LQR designed in section 6.2.1 and the bang-bang controller designed in section 6.2.2. A summary of the 135 runs as heave and pitch RAOs for these three cases at these three speeds are given in figures 6.1, 6.2, 6.3, 6.4, 6.5 and 6.6. For each of the points, a number of identical runs were performed, and the $\pm\sigma$ uncertainty bounds are represented by the error bars shown.

The average added resistance due to waves with these three control strategies is given as a percentage in figure 6.7. These values should be taken as approximations only, as full resistance tests were not carried out in smooth water for comparison.

The following can be noted from the initial control testing:

- Significant reduction in the pitch and heave motions is achievable with the control system;
- At high frequencies, both control systems are not fast enough, although the bang-bang controller does have the advantage of 'preempting' the motions;
- The LQR results are not only generally better than the bang-bang control results, but they also show better consistency, as can be seen by the $\pm\sigma$ bounds shown.

Further discussion of these results is included in section 6.4.

The results of the revised LQR design are now presented. They are compared to the results above in figures 6.8, 6.9, 6.10 and 6.11, displaying them in terms of the bow and stern motions and accelerations rather than the heave and pitch of the vessel. From these, several points can be noted:

- Even though the results plotted as heave and pitch RAOs showed that the LQR was the best controller overall, when these are plotted according to bow and stern results, this is not so clear. It can be seen that for low frequencies, the accelerations at the bow are more damped by the LQR controller. However, at the stern, it can be seen that the bang-bang controller is consistently better at reducing the motion and accelerations. This is probably due to the fact that the control surface is at the stern, and the bang-bang controller responds more sharply to a disturbance at that point than the LQR controller.
- The responses at the bow and stern are not better damped by an LQR controller based on the positions or velocities at these points, as compared to the LQR controller based on heave and pitch. In some cases, they are significantly worse.

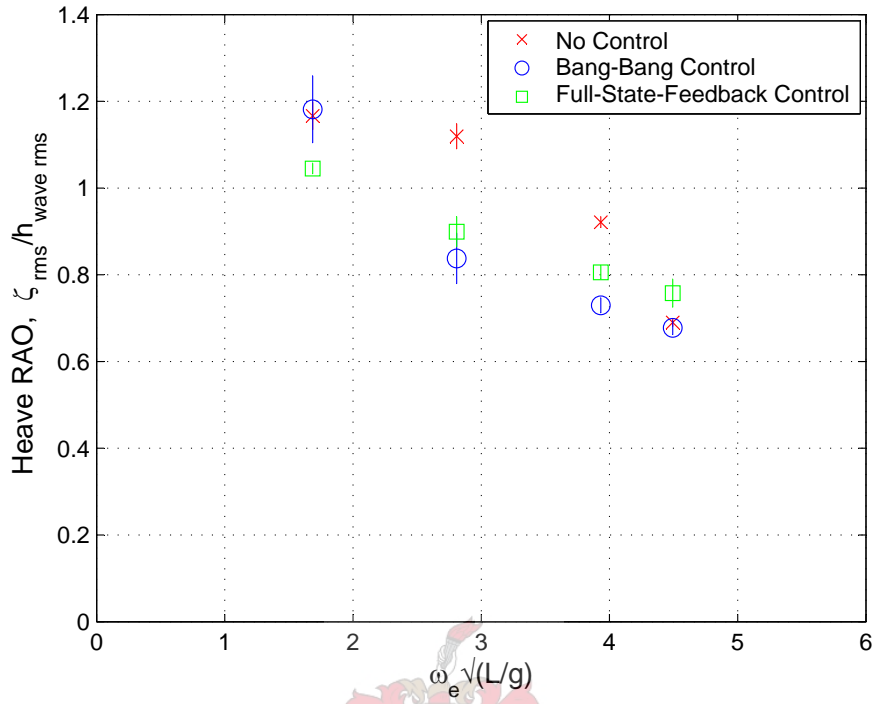


Figure 6.1: Controlled heave RAO comparison for initial three strategies, 4 m/s

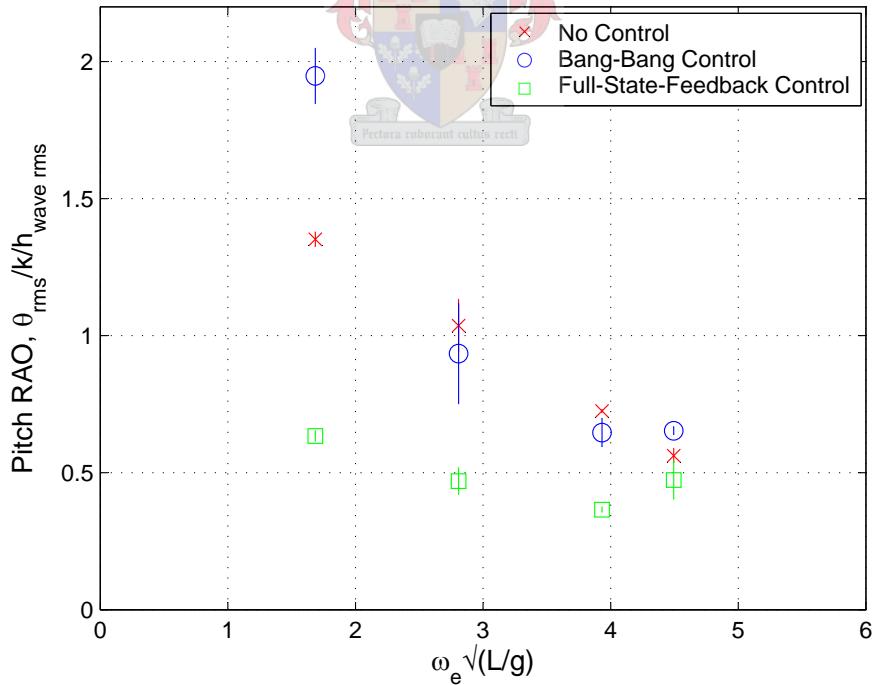


Figure 6.2: Controlled pitch RAO comparison for initial three strategies, 4 m/s

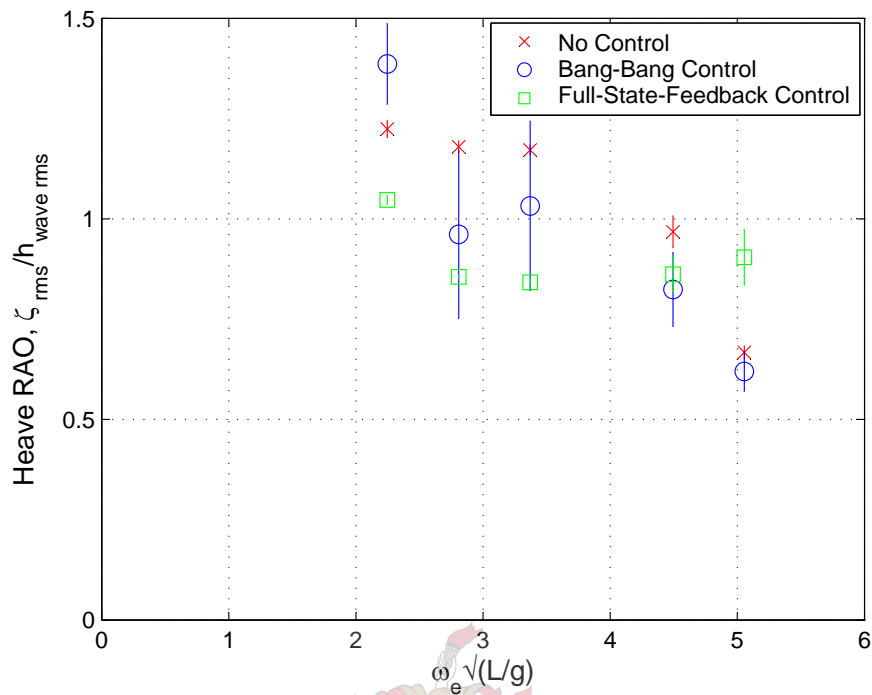


Figure 6.3: Controlled heave RAO comparison for initial three strategies, 5 m/s

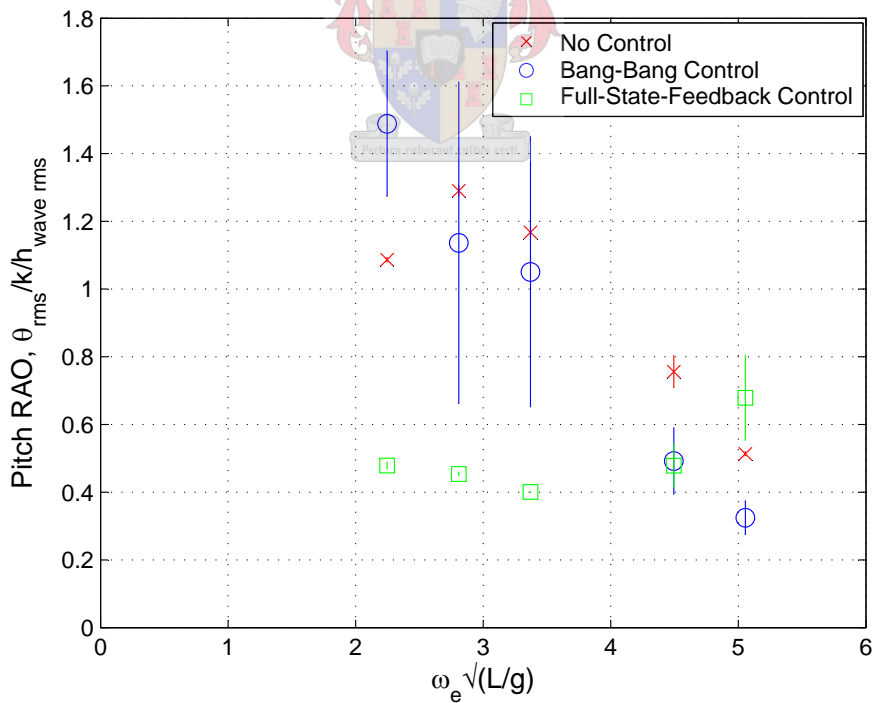


Figure 6.4: Controlled pitch RAO comparison for initial three strategies, 5 m/s

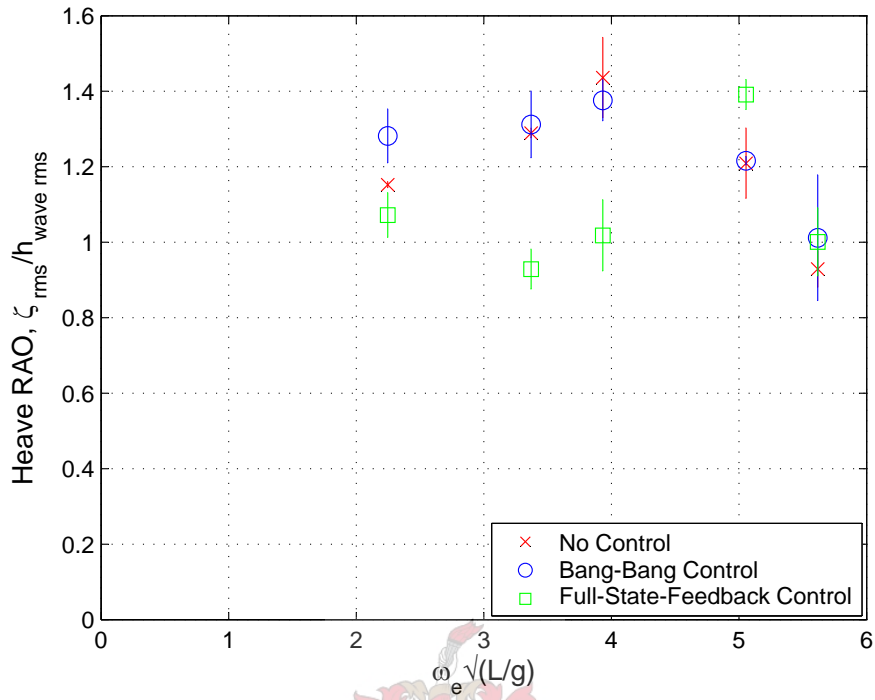


Figure 6.5: Controlled heave RAO comparison for initial three strategies, 6 m/s

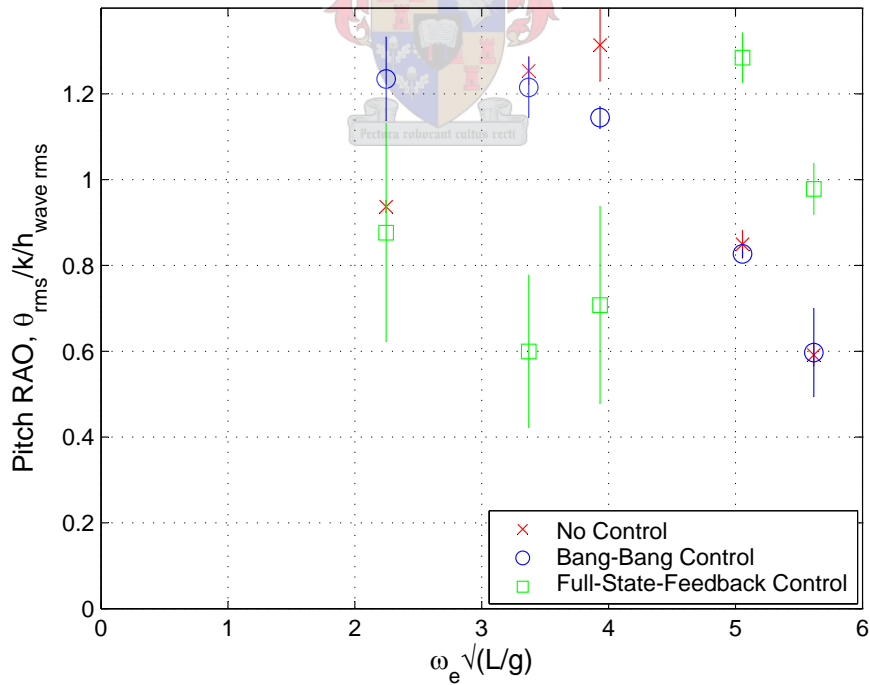


Figure 6.6: Controlled pitch RAO comparison for initial three strategies, 6 m/s

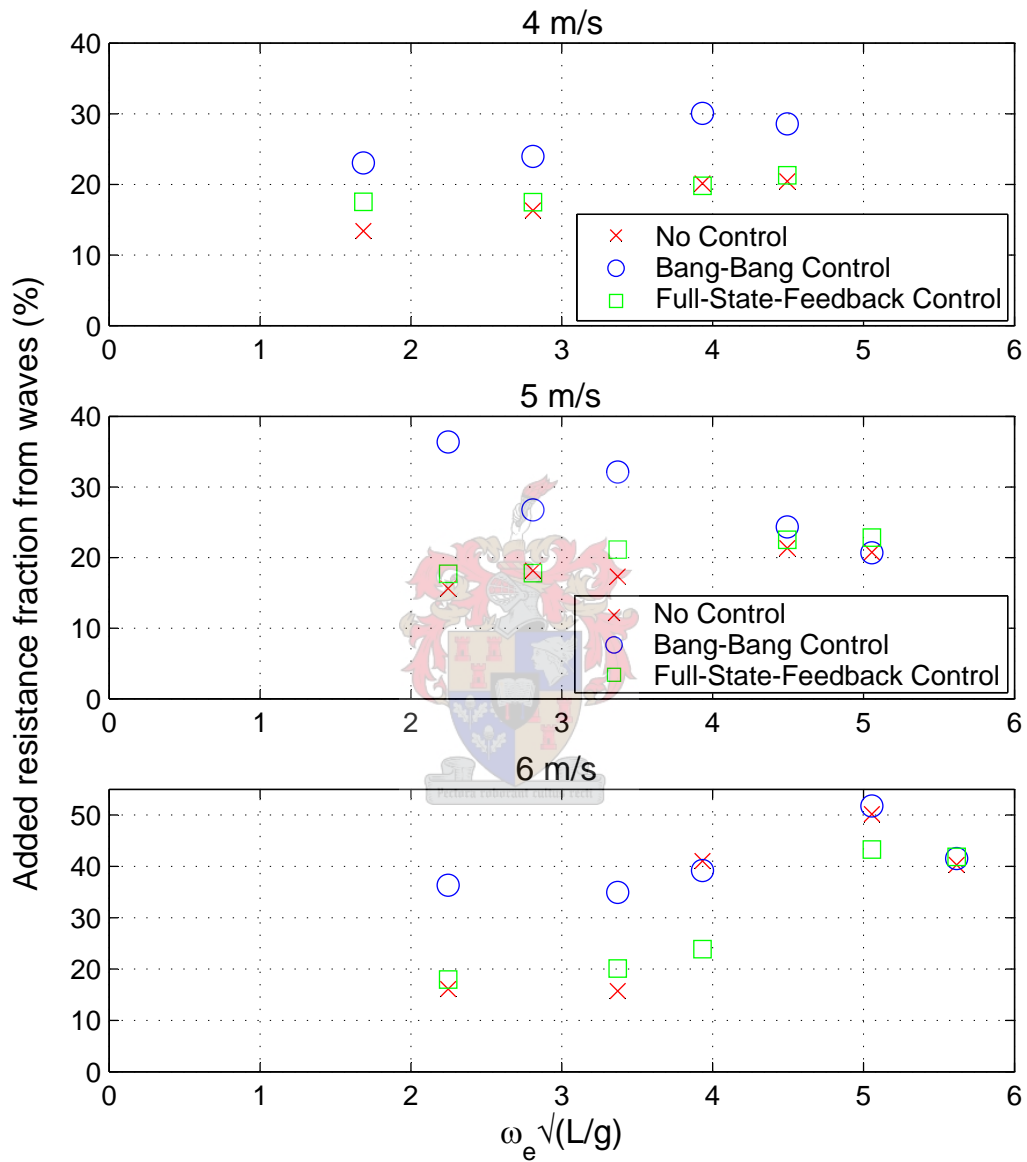


Figure 6.7: Added resistance fraction due to waves for initial three control strategies at 4,5, and 6 m/s

- The additional points from the two revised LQR controllers tend to lie close to one another. This indicates that minimising the bow and stern motions has similar results to minimising their velocities.

6.4 Discussion and conclusions

From the results presented in the previous section, it can be seen that the control systems implemented generally provided significant improvements in the motions of the model vessel. The results presented demonstrate the following:

- Overall, the LQRY controller based on the heave and pitch seems to be best at reducing the wave-induced motions of the vessel. This is because:
 - The heave and pitch motions are reduced to a greater degree across the board. For the stern motions, the bang-bang controller performed better, however, meaning that specific criteria might not be best with the LQR controller.
 - This is despite the fact that it is more delayed than the bang-bang controller;
 - The added resistance is lower in almost all cases. The only exception is at high frequencies, where the system was not quick enough to keep up;
 - Visually, the stability of the system is better with this design;
 - The design is easier and more reliable; only one set of calculated gains is used for all cases. For the bang-bang controller, the phase and step sizes must be chosen carefully.
- As expected in its design, the control system's speed was an important limitation to its performance at high frequencies. The time delay for the formation of lift on the control foil is also important, but less so because it has a relatively large control authority for this size vessel;

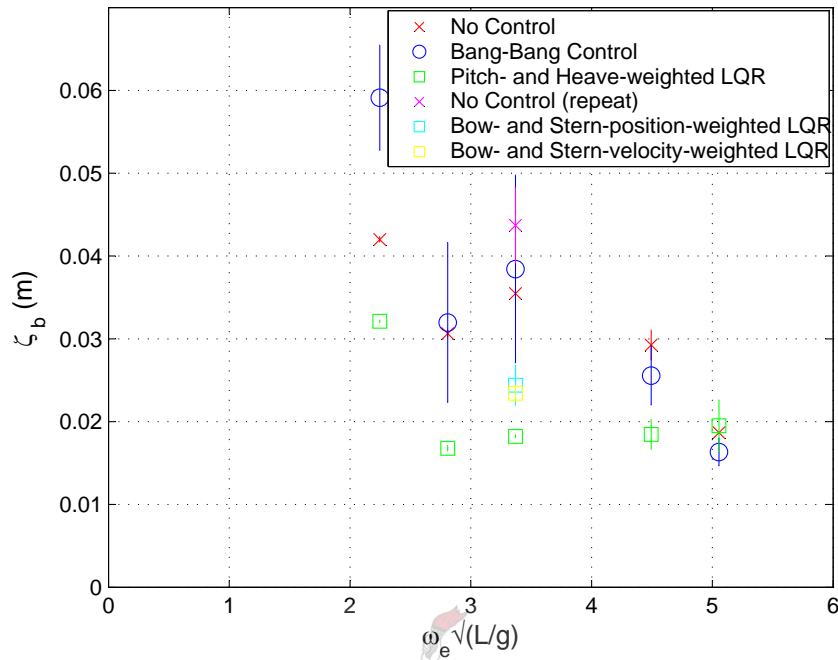


Figure 6.8: Bow vertical position responses for all five control strategies tested

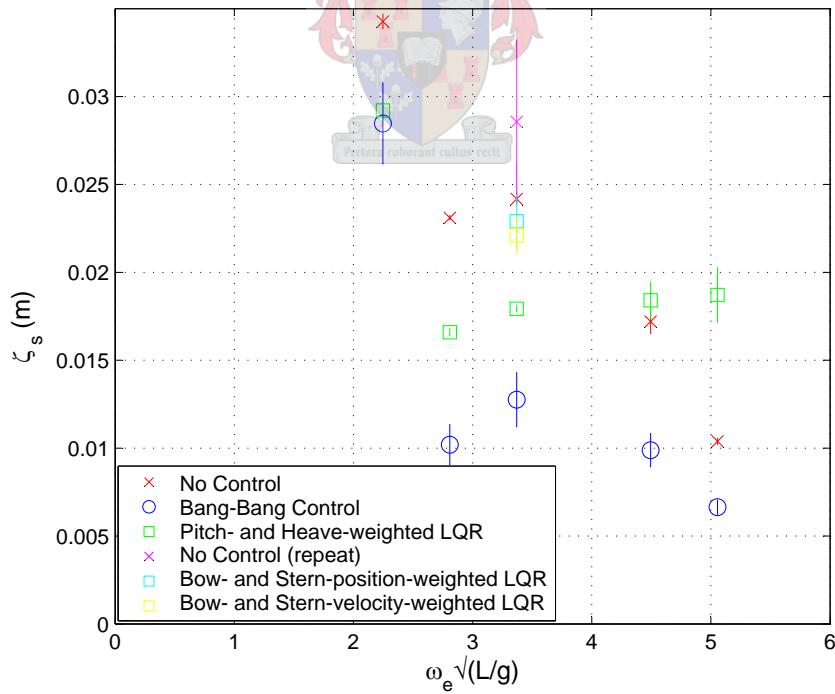


Figure 6.9: Stern vertical position responses for all five control strategies tested

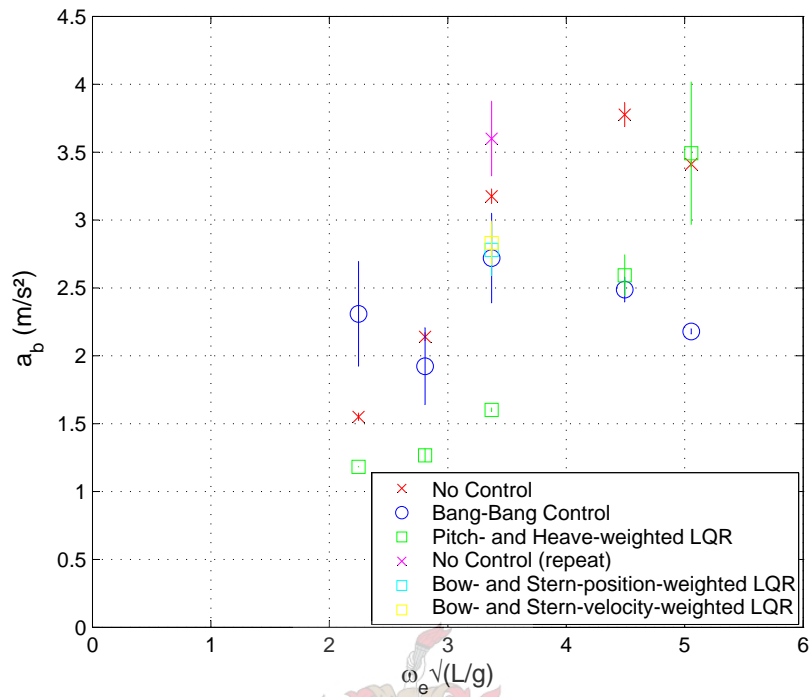


Figure 6.10: Bow acceleration responses for all five control strategies tested

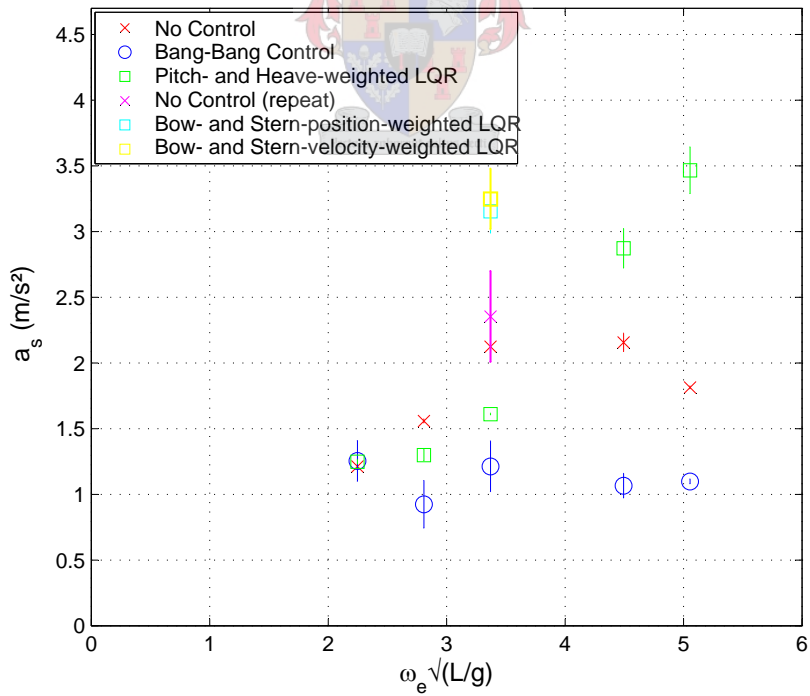


Figure 6.11: Stern acceleration responses for all five control strategies tested

- The inclusion of fences was important in blocking ventilation and obtaining a good lift response from the foils in quickly-variable angle situations;
- The foil angle's limitation seemed to be more from the speed of the system than the maximum allowable stall angle;
- Revision and attempted optimisation of the LQR controller indicates that the results observed are about the best obtainable with this system.



Chapter 7

Conclusions

In the preceding chapters, the modelling of the vertical motions of a HYSUCAT system was given, as well as design of several controllers to reduce these motions. The primary conclusions that can be drawn from this study are as follows:

Simple strip methods, such as the one applied in POWERSEA, are inadequate to accurately model the seakeeping of a HYSUCAT for all but low planing speeds. Seakeeping calculations were carried out using a strip method for the planing hull, and using the Peter du Cane theory to simulate the foils. Results obtained as compared to experimental towing tank runs are given in section 3.4, particularly in figures 3.1 and 3.2. The agreement with measurements from tank tests was fair at low speeds, but deteriorated as the planing speed increased. Thus, in a seakeeping design, this highlights the primary limitation of this method, and the advantage of using a modelling method which is able to simulate in more detail. Also noted in section 3.5 from the results is the lack of agreement in the pitch results at low frequencies, as predicted by the literature.

In addition to this, indication was given that the steady-state Peter du Cane lift model must be used with caution when simulating vessels in waves, as it does not capture various time-dependent flow effects and was designed primarily for steady-state foil behaviour.

A useful linear model of the vertical motions of a HYSUCAT can be obtained using appropriate experimental system identification techniques. In section 4.1, a simple model of the vertical motions of the HYSUCAT was proposed. This was tested experimentally, and representative values were found to model the system well using a parameter estimation technique used extensively in the aerospace industry. This was for a range of speeds and disturbance amplitudes, capturing the system's primary dynamics about the operating point. See section 4.2.2 for plots of the parameter values obtained, as well as section 4.2 for more information on the method and its assumptions.

A simply-designed controller can be practically implemented in real time to dramatically reduce the pitch and heave motions of a HYSUCAT model in regular waves. Various controller designs were implemented in real time on a HYSUCAT model, in order to reduce the pitch and heave motions. For the pitch motions, rms motion reductions were seen of 65% at the design point, and typical values of 50% (see figure 6.4) using the output-weighted LQR as compared to no control. For the heave motions, a reduction of 32% was realised at the design point, and typically 20% for general frequencies. See figure 6.4 for these results. Thus a control and foil system with sufficient response speed in real-time can be designed and implemented to practically reduce the motions of a representative HYSUCAT in regular waves.

7.1 Further work

As this was the first work that investigates improving the seakeeping of HYSUCATs, much scope is available for further research in this important area. Some suggestions for theoretical work, attempting to better model and verify the detailed flow of a vessel and foils in waves are:

- Investigate the correlation of POWERSEA predictions to tank tests for a HYSUCAT with the foils removed, in order to check the degree to which the foil model caused the poor results experienced in this project. This

would also highlight limitations in the strip theory used, especially at high speeds;

- Using a more detailed time-dependent model of the foil lift, use the custom C-code add-ins in POWERSEA to improve the representation of the foils;
- Test the foils (possibly individually) in waves using load cells to determine the lift forces developed, as well as the effect of the wave orbital velocity on this lift. See Kim & Yamato (2003) for an example;
- Perform further system identification tests in an attempt to explain and model the significant nonlinearities present in the system, also determining the extent to which a linearised model can practically be used;
- Test more complex control strategies to compensate for the time delays of the system, such as disturbance estimation. In this, the vessel detects the upcoming waves in real time, either by direct measurement from the bow or by estimation from the vessel's own motions. It then estimates the predictable component of the disturbance (see for example Franklin *et al.* (1998) and Kim & Yamato (2004)) to improve the disturbance rejection of the system, estimating the disturbance from the dominant frequency of the waves.

For practical work, where the focus is on producing a workable ride control system for a full-scale vessel, the following are recommended:

- Tailor the control design so that it can be fully implemented on board the vessel, as it would in a full-scale vessel;
- Investigate simplifying the controller design for implementation purposes;
- Design appropriate robust hardware to allow for the scaling of the system used here to a full-scale vessel.

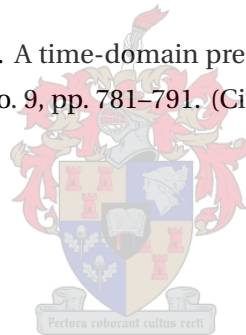
Bibliography

- Akers, R. (1998). *POWERSEA Reference Manual and Tutorial, Version 4.0*. Ship Motion Associates. (Cited on pages 21 and 29.)
- Arri, T., e.a. (1993). Development of ship motion control system for hybrid hydrofoil catamaran 'superjet-30'. *Hitachi Zosen Technical Review*, vol. 54, pp. 36–41. (Cited on page 6.)
- Bertorello, C. (2001). Design trends of small size fast passenger ferries. In: *HIPER '01 conference proceedings*. (Cited on page 1.)
- Bertram, V. (2000). *Practical Ship Hydrodynamics*. Butterworth Heinemann. (Cited on pages 11, 12, and 16.)
- Bhardwaj, S. (2004 January). *Active Ride Control System for High Speed Planing Craft*. Masters, Stevens Institute for Technology, New York. (Cited on page 19.)
- Browne, K. (2005 June). Personal Interview. Stellenbosch. (Cited on page 35.)
- Constantinescu, A., e.a. (2004). Hydro-elastic simulation of simple 2-d geometries in water entry. In: *HIPER '04 Conference Proceedings*. (Cited on page 2.)
- du Cane, P. (1972). *High Speed Small Craft*. David & Charles: Newton Abbot. (Cited on pages 6 and 17.)
- Faltinsen, O. (1990). *Sea Loads on Ships and Offshore Structures*. Cambridge University Press. (Cited on page 12.)
- Fossen, T.I. (1994). *Guidance and Control of Ocean Vehicles*. John Wiley & Sons, Chichester. (Cited on page 16.)

- Franklin, G.F., Powell, J.D. and Workman, M. (1998). *Digital Control of Dynamic Systems*. 3rd edn. Addison Wesley Longman, Inc, Menlo Park, CA. (Cited on pages 61 and 76.)
- Griffin, M.J. (1990). *Handbook of Human Vibration*. Academic Press, Ltd, London. (Cited on page 14.)
- Haddara, M.R. and Xu, J. (1997 November). On the identification of ship coupled heave-pitch motions using neural networks. *Ocean Engineering*, vol. 26, pp. 381–400. (Cited on pages 17 and 18.)
- Houghton, E.L. and Carpenter, P. (1993). *Aerodynamics for Engineering Students*. 4th edn. Arnold: London. (Cited on pages 23 and 53.)
- Inman, D.J. (2001). *Engineering Vibration*. 2nd edn. Prentice-Hall, Inc, Upper Saddle River, NJ. (Cited on page 38.)
- ISO (1997). *2631-1, Mechanical vibration and shock - Evaluation of human exposure to whole-body vibration - Part 1: General Requirements*. International Organisation for Standardization, 2nd edn. (Cited on page 14.)
- Kihara (2004). Numerical models of water impact. In: *HIPER '04 Conference Proceedings*. (Cited on page 2.)
- Kim, S. and Yamato, H. (2003). An experimental study of the longitudinal motion control of a fully submerged hydrofoil model in following seas. *Ocean Engineering*, vol. 31, pp. 523–537. (Cited on pages 17 and 76.)
- Kim, S.-H. and Yamato, H. (2004). On the design of a longitudinal motion control system of a fully-submerged hydrofoil craft based on the optimal preview servo system. *Ocean Engineering*, vol. 31, pp. 1637–1653. (Cited on pages 19 and 76.)
- Lewis, C.H. and Griffin, M.J. (1997). Evaluating the motions of a semi-submersible platform with respect to human response. *Applied Ergonomics*, vol. 28, no. 3, pp. 193–201. (Cited on page 14.)
- Ma, S., Duan, W.-Y. and Song, J.-Z. (2004 June). An efficient numerical method for solving 2.5d ship seakeeping problem. *Ocean Engineering*, vol. 32, no. 8-9, pp. 937–960. (Cited on page 12.)

- Maine, R.E. and Iliff, K.W. (1986 June). Application of parameter estimation to aircraft stability and control: The output-error approach. Reference publication, NASA. (Cited on page 34.)
- Matveev, K. and Matveev, I. (2000 January). Tandem hydrofoil system. *Ocean Engineering*, vol. 28, no. 2, pp. 253–261. (Cited on page 5.)
- Milne, G.W. (2000). *MMLE-3 Identification Toolbox for State-Space System Identification using MATLAB*. Version 1.3 and 1.4. (Cited on page 34.)
- O'Hanlon, J.F. and McCauley, M.E. (1974). Motion sickness incidence as a function of the frequency and acceleration of vertical sinusoidal motions. *Aerospace Medicine*, vol. 45, no. 4, pp. 366–369. (Cited on page 14.)
- Payne, P. (1995). Contributions to planing theory. *Ocean Engineering*, vol. 22, no. 7, pp. 699–729. (Cited on page 8.)
- Payne, P.R. (1988). *Design of High Speed Boats - Planing*. Fishergate, Inc., Maryland. (Cited on pages 7 and 8.)
- Pienaar, L.d.V. and Roos, H. (1991 November). *Ship Model Tests in Waves*. Final Year Thesis, Department of Mechanical Engineering, Stellenbosch University. (Cited on page 2.)
- Santos, M., López, R. and de la Cruz, J. (2004). Fuzzy control of the vertical acceleration of fast ferries. *Control Engineering Practice*, vol. 13, pp. 305–313. (Cited on page 18.)
- Savitsky, D. and Koelbel, J.G. (1993 June). Seakeeping of hard chine planing hulls. Technical and Research Bulletin R-42, Society of Naval Architects and Marine Engineers (SNAME). (Cited on page 29.)
- The MathWorks, I. (2003). *MATLAB® product help files, R13*. (Cited on page 61.)
- van Walree, F. (1999 March). *Computational Methods for Hydrofoil Craft in Steady and Unsteady Flow*. Ph.D. thesis, Technische Universiteit Delft, Wageningen, Netherlands. (Cited on pages 5 and 6.)
- Wagner, H. (1932). Über stoss- und gleitvorgänge an der oberfläche von flüssigkeiten. In: *Zeitschrift für Angewandte Mathematik und Mechanik*. (Cited on page 8.)

- Welnicki, W. (1998 Septembera). The enhancement of seakeeping qualities of fast catamaran by means of stabilizing foils. *Polish Maritime Research*, vol. 5, no. 3(17), pp. 10–13. (Cited on page 15.)
- Welnicki, W. (1998 Septemberb). The influence of fixed foils on sea keeping qualities of fast catamaran. In: *Proceedings of the 7th International Symposium on Practical Design of Ships and Mobile Units*. The Hague, The Netherlands. (Cited on page 15.)
- Wertheim, A.H., Bos, J.E. and Bles, W. (1999 March). Contributions of roll and pitch to sea sickness. *Brain Research Bulletin*, vol. 47, no. 5, pp. 517–524. (Cited on page 15.)
- Zarnick, E. (1978 March). A nonlinear mathematical model of motions of a planing boat in regular waves. Tech. Rep. DTNSRC-78/032, David W. Taylor Naval Ship Research and Development Center, Bethesda, Maryland 20084. (Cited on pages 2, 20, and 21.)
- Zhu, D.X. and Katory, M. (1998). A time-domain prediction method of ship motions. *Ocean Engineering*, vol. 25, no. 9, pp. 781–791. (Cited on page 11.)



Appendices



Appendix A

Model HYSUCAT measurement and POWERSEA settings

A.1 Hull form measurement and simplification

In order to input the vessels existing shape into POWERSEA, the form of the hulls was measured up.

The POWERSEA seakeeping program only accepts two hull lines in its description of the model - the keel and main chine lines. Between these two, the deadrise angle is created using a straight line. It is also assumed that the chine is sharp, which means that the hull surface above the main chine line is dry. The catamaran, as can be seen from the figure given, is largely made up of flat surfaces and has a single hard chine, which means that these assumptions are not unreasonable. Thus the two small chines at the bow of the vessel had to be ignored because of these limitations in the computer program. However, they are not seen to be large enough to have caused significant differences in the two models.

For measurement of the hulls, a measuring table was used, on which one of the hulls was laid. The chine and keel lines were the measured using a height gauge at different grid positions from the flat surface. The measured points used are given in tables A.1 and A.2.

Table A.1: Measured model keel line points

#	x	y	z
1	0.000	0.000	0.000
2	-0.165	0.000	0.000
3	-0.330	0.000	0.000
4	-0.497	0.000	0.000
5	-0.663	0.000	0.000
6	-0.829	0.000	0.000
7	-0.904	0.000	0.000
8	-1.000	0.000	0.003
9	-1.050	0.000	0.005
10	-1.100	0.000	0.008
11	-1.125	0.000	0.011
12	-1.150	0.000	0.013
13	-1.175	0.000	0.018
14	-1.200	0.000	0.023
15	-1.225	0.000	0.034
16	-1.250	0.000	0.045
17	-1.275	0.000	0.063
18	-1.300	0.000	0.093
19	-1.325	0.000	0.110
20	-1.350	0.000	0.136
21	-1.471	0.000	0.303

Table A.2: Measured model main chine line points

#	x	y	z
1	0.000	0.129	0.053
2	-0.165	0.129	0.053
3	-0.330	0.129	0.055
4	-0.497	0.128	0.056
5	-0.663	0.128	0.059
6	-0.829	0.127	0.064
7	-0.904	0.126	0.071
8	-0.996	0.122	0.089
9	-1.073	0.116	0.100
10	-1.163	0.102	0.118
11	-1.240	0.084	0.138
12	-1.330	0.048	0.164

A.2 Model parameter experiments

Simple experiments were carried out to determine the physical parameters of the model. The vessel was suspended from an axis parallel to the pitching y-axis by four lines to the bow and stern. A plumb bob was then used to draw a vertical line from this axis through the centre hanging directly below it. This was done for the model at different 'pitch' angles, and from this the vertical and horizontal centre of gravity could be determined.

For the radius of gyration experiments, the following derivation is used:

Using Newton's 2nd law or energy methods, the equation of motion of the model can be shown to be

$$I_{OO}\ddot{\theta} - lmg \sin(\theta) = 0 \quad (\text{A.2.1})$$

Using the small angle approximation that $\sin(\theta) = \theta$, this can be written as

$$I_{OO}\ddot{\theta} - lmg\theta = 0 \quad (\text{A.2.2})$$

By analogy to a mass-spring system, which has equation

$$m\ddot{x} - kx = 0 \quad (\text{A.2.3})$$

and $\omega_n = \sqrt{k/m}$, it can be seen that

$$\omega_n = \sqrt{\frac{lmg}{I_{OO}}} \quad (\text{A.2.4})$$

which can also be written as $I_{OO} = \frac{lmg}{\omega_n^2}$.

The moment of inertia can be transferred from the axis at the centre of rotation OO to the centre of gravity GG using the parallel axis theorem. This states that

$$I_{GG} = I_{OO} - ml^2 \quad (\text{A.2.5})$$

Using this and the fact that the radius of gyration $r_G = \sqrt{I_{GG}/m}$, the sub-

stitution yields

$$r_G = \sqrt{\frac{\frac{lmg}{\omega_n^2} - ml^2}{m}} \quad (\text{A.2.6})$$

All the unknowns in equation A.2.6 above are measurable by weighing and pendulum experiments, and can be substituted into the equation above. For pendulum experiments, ω_n is obtained by suspending the model, with mL the distance between the centre of gravity and centre of rotation, and swinging it in the pitching direction. The frequency measured is ω_n .

A.3 POWERSEA input settings

The following is a description of the inputs used in the POWERSEA program. Italicized commands such as *Boat->Vessel Params* indicate the inputs that are discussed are situated in the 'Vessel Params' GUI under the 'Boat' pull-down menu in POWERSEA. For the model parameters given in *Boat->Vessel Params*, description of experiments done are given in appendix A.2. The values used are given in table 3.1.

For the empirical vessel coefficients in *Boat->Vessel Coefficients*, the automatically generated coefficients were used. For the residual forces setting, each time a new speed was set, the vessel was run in smooth water using 'Calculate Residual Forces', and then set to 'Use Precalculated Residual Forces' for the remainder of the wave simulations at that speed. This is given in the program help files, but is unclear and was checked with the author.

For *Boat->Propulsion* settings, 'Effective Power or Thrust' was the propulsion type, the propulsion location and angle was entered (see table 3.1), 'Tank Test Mode' was selected and the 'Thrust Control Location' was 'No Point Specified'. These were chosen because in the towing tank, the effective thrust is always provided at the given point, regardless of the motions of the model.

Boat->Simulation Properties were set with the 'Longitudinal Force Correction' ON, and the Savitsky empirical models were set OFF.

Conditions->Initial Conditions are not very important in the steady state response of the vessel, and were mostly set using the program's built in 'Hy-

drostatic Analysis' tool, which makes an estimate of the zero speed trim and draft of the vessel. 'Surge Velocity' was set to the forward velocity, which means that the vessel has the same speed for the entire run.

Conditions->Incident Waves gave the option of using one of the standard input distributions such as the Pierson-Moskovich, ITTC or JONSWAP distributions (see section 2.6 for more information). For this project, only 'Calm Water' and 'Regular Waves' settings were used, with the standard 1 second ramp up time to improve convergence. For the waves, 'Head Seas' were used (as in the towing tank) and the wave height and wavelength were defined as given in section 2.6.

For the inputs of *Conditions->Thrust/Propulsion Conditions*, the propulsion mode was a constant velocity, which depended on the particular run being performed.

In the *Analysis* menu, *Analysis->Simple Hydrostatics* was run when necessary to get reasonable initial conditions and to check that the model was performing as expected at zero speed. In the *Analysis->Run Control* settings, the 'Stop Time' and 'Time Step' were adjusted from recommended values given by the 'Preset' button. Usually the time step could be doubled with no influence on the results, and to reduce the amount of data produced, the 'Stop Time' was often shortened as necessary. *Analysis->Simulation Tolerances* were left at their default settings, except for the tests described in section 3.3.


Appendix B

Peter du Cane hydrofoil theory

The 'Peter du Cane' theory for lift and drag of three dimensional foils is given below. The details here are repeated because the source (du Cane 1972) is out of print and not widely available, and are sufficient for use of the theory. Full details, as well as motivation and discussion can be found in pp33 – 41 of

B.1 Hydrofoil lift

The lift equation used in this theory is the well-known


$$C_{L0} = \frac{1}{2} \rho V^2 S C_L, \quad (\text{B.1.1})$$

which is proportional to the fluid density ρ , the planform area S , the lift coefficient C_L and the square of the velocity (V^2). The theoretical maximum value for C_L is $C_{L0} = 2\pi\alpha_T$, where α_T is the relative angle of attack measured from the angle at which no lift is generated.

B.2 Hydrofoil drag

The drag of a hydrofoil can be similarly treated, using

$$D = \frac{1}{2} \rho V^2 S C_D, \quad (\text{B.2.1})$$

where D , the drag coefficient, replaces C_L above. Very little of the drag is due to viscous effects; most of the drag is 'parasitic drag' due to the lift vector being tilted back from the vertical.

In the absence of experimental data for a foil, an estimate of the section drag coefficient can be obtained by the empirical expression

$$C_{D0} = 2C_f(1 + 1.2t/c) + 0.11(C_L - C_{L1})^2 \quad (\text{B.2.2})$$

where C_{L1} is the lift coefficient for which the section is designed, and C_f is the flat plate friction coefficient commonly used in fluid dynamics. An empirical conservative estimate for C_f for 'rough' surfaces has been given by Hoerner???? in the form,

$$C_f = 0.032(k/c)^{1/5} \quad (\text{B.2.3})$$

where k is the 'average height of the surface roughness' and c is the chord length.

Most of the other drag forces experienced by a foil are due to the lift vector varying from the design value, causing an additional drag coefficient $\Delta C_L = C_L \Delta\alpha$, which is more conveniently written

$$\frac{\Delta C_D}{C_L^2} = \frac{\Delta\alpha}{C_L} \quad (\text{B.2.4})$$

for addition to the final drag equations.

B.3 Free-surface effects

One of the main differences between a hydrofoil and an aerofoil is the presence of hydrofoil free-surface effects. The low pressure caused above the foil causes a distortion of the water surface to try and relieve it, which in turn reduces the lift that can be achieved with the foil at that depth.

This effect is relatively complex, but a reasonable approximation can be made by including two factors, namely

- the lift loss due to pressure relief as a function of foil depth, calculated

at an infinite Froude number,

- the change in angle of the lift vector due to the wave effect, as a function of foil depth and Froude number.

The first effect can be approximated by multiplying the inverse lift-curve slope by K , where

$$K = \frac{(4h/c)^2 + 1}{(4h/c)^2 + 2}. \quad (\text{B.3.1})$$

This lift loss is about 5% at a depth of one chord, but increases to 50% at the surface, which means the foil has become a planing surface - this lift curve slope is π for infinite span.

The free-surface wave effect affects the lift, and thus also the drag of the foil. It can be approximated using

$$\Omega = \frac{\alpha_w}{C_L} = \frac{C_{DW}}{C_L^2} = \frac{1}{2F^2} \exp(-2h/(cF^2)), \quad (\text{B.3.2})$$

where h/c is the ratio of foil submergence to chord length and F is the Froude number, $F = \sqrt{gc}$.

B.4 Finite span effects

As in aerodynamics, the finite span of the foil incurs further losses due to the trailing vortices formed at the tips. This is in the form of lift losses due to a change in the effective angle of attack, as well as an induced drag component. Using the elliptical loading profile, the theoretical optimum, a wing with aspect ratio A has an induced lift angle and drag component given by

$$\frac{\alpha_1}{C_L} = \frac{C_{D1}}{C_L^2} = \frac{1 + \sigma}{\pi A} \quad (\text{B.4.1})$$

σ is Prantl's finite-span biplane factor, which is based on the fact that the free surface effect on a finite span is very similar at high Froude numbers to biplane interference effects. A reasonable approximation for σ for these pur-

poses is given by

$$\sigma = \frac{A}{A + 12h/c} \quad (\text{B.4.2})$$

In addition to the above, modest aspect ratios require an additional multiplication of the inverse lifting line factor $1/2\pi$ by a factor E, for which a simple experimentally determined empirical equation is

$$E = 1 + 2/A^2 \quad (\text{B.4.3})$$

B.5 Planform, strut and geometry effects

The above effects are also dependent on the particular geometry of the foil. If there is any angle of sweep λ or dihedral Γ , they are dealt with by multiplying the lift curve slope by $\cos \lambda$ or $\cos \Gamma$, respectively.

For strut and surface piercing foil effects, the aspect ratio is modified according to the following

For struts:

$$A = \frac{b}{c} \left[1 + \left(\frac{a}{b} \right)^3 \frac{h}{b} \right] \quad (\text{B.5.1})$$

where a is the distance between struts, b is the foil width, c is the chord length and h the submergence.

For surface piercing foils, i.e. with dihedral,

$$A = \frac{b}{c} \left(1 + \frac{h}{b} \right) = \frac{h}{c} (1 + 4 \cot \Gamma) \quad (\text{B.5.2})$$

with the same definitions as in B.5.1 above.

B.6 Lift and drag summary

Collecting all the above components, the lift and drag of a hydrofoil can be approximated by

$$\frac{\alpha_T}{C_L} = \frac{1/K + 2/A^2}{2\pi \cos \lambda \cos \Gamma} + \Omega + \frac{1 + \sigma}{\pi A} \quad (\text{B.6.1})$$

$$\frac{C_D}{C_L^2} = \frac{C_{D0}}{C_L^2} + \Omega + \frac{1 + \sigma}{\pi A} \quad (\text{B.6.2})$$

where

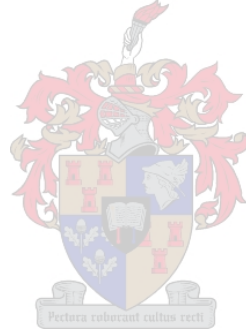
- K is given by eq. B.3.1,
- Ω is given in eq. B.3.2 and is a function of (h/c) and Froude number,
- σ is a function of depth ratio (h/c) and A , and is given by B.4.2
- and A is the effective aspect ratio given in equations B.5.1 and B.5.2.



Appendix C

Control mechanism drawings

Included here are the engineering drawings of the controllable trim foil mechanism. The hardware design motivation and description is provided in 5.3.1.



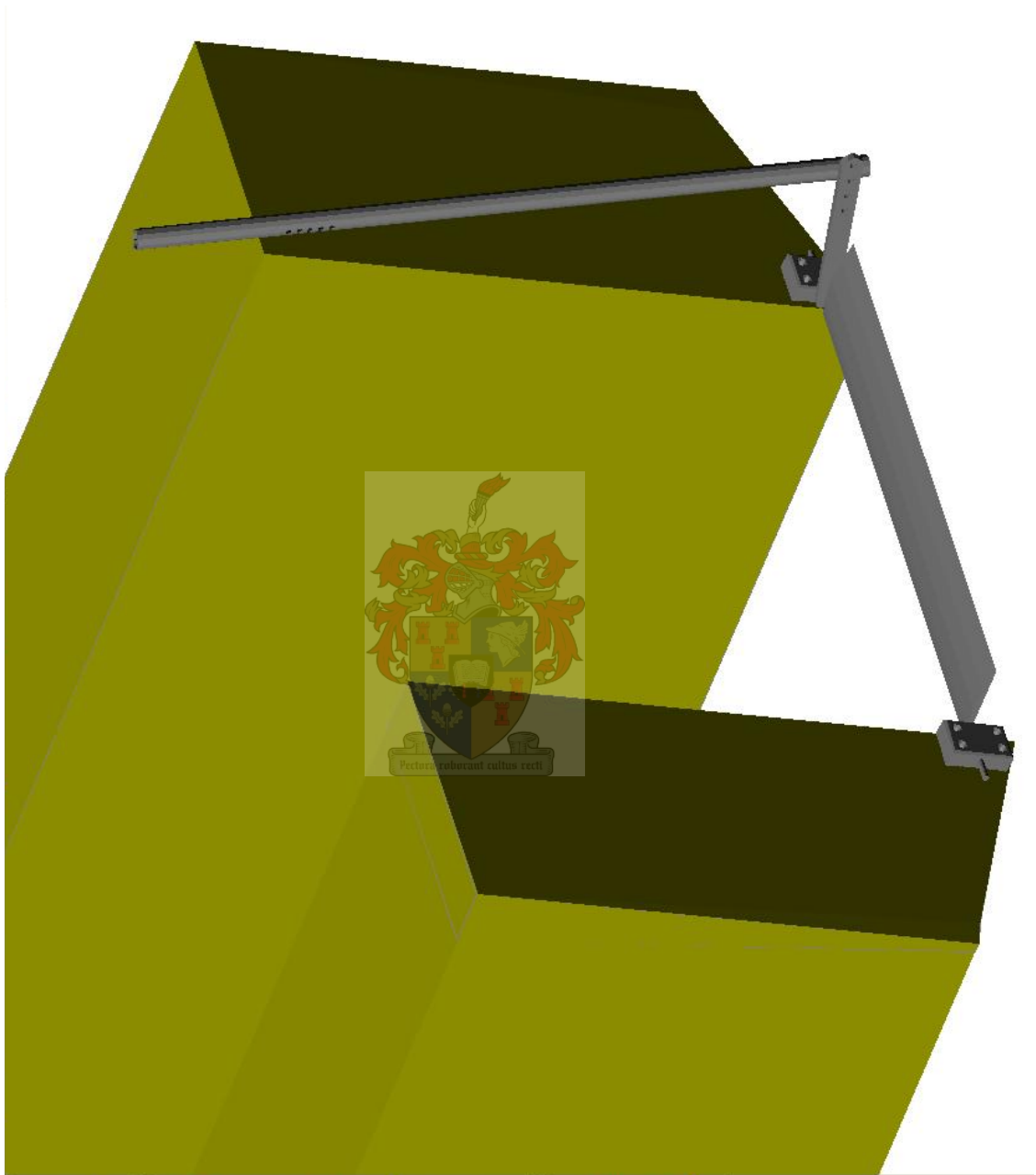


Figure C.1: Isometric view of mechanism assembly

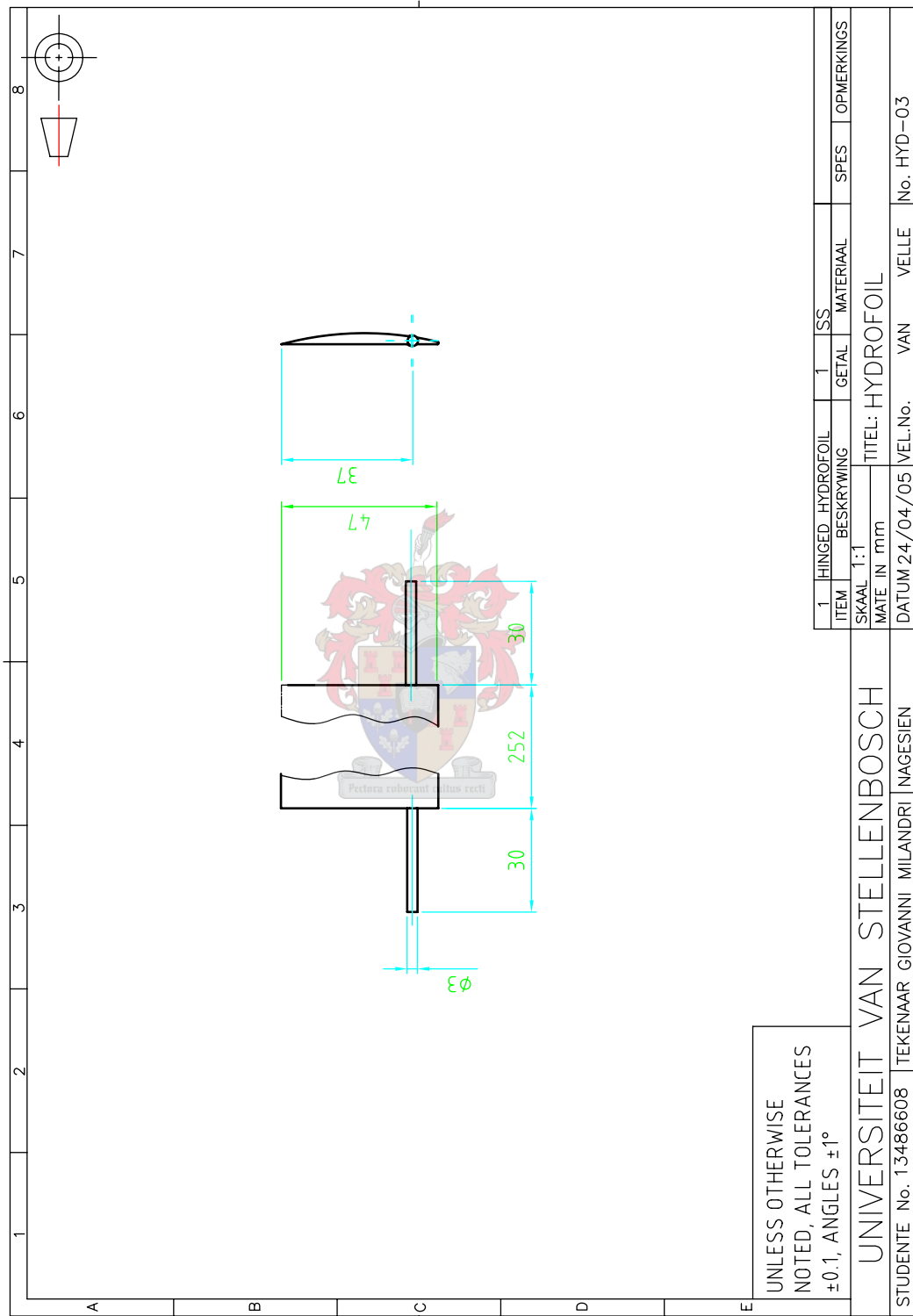


Figure C.2: Hinged hydrofoil drawing

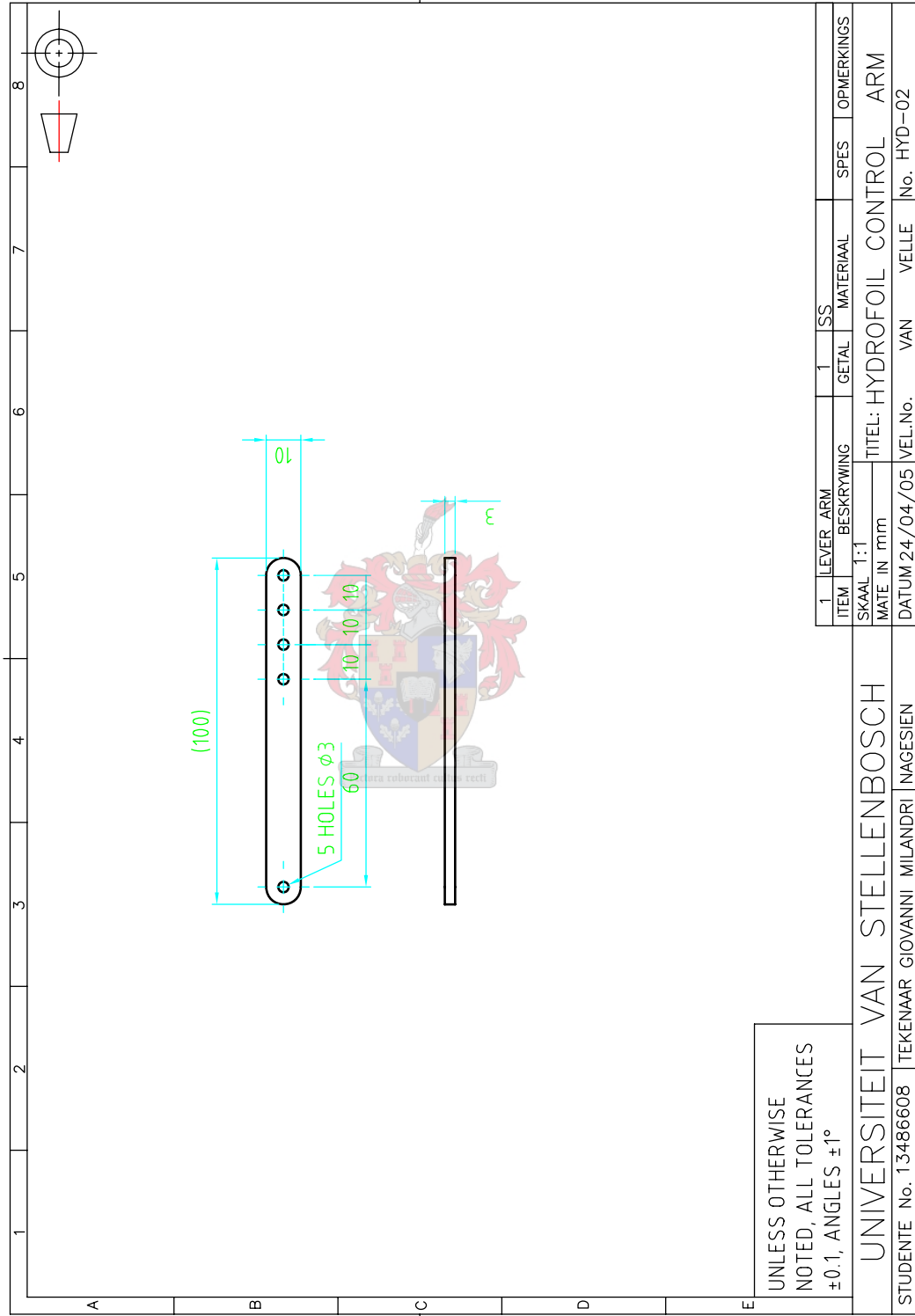


Figure C.3: Hydrofoil control arm drawing

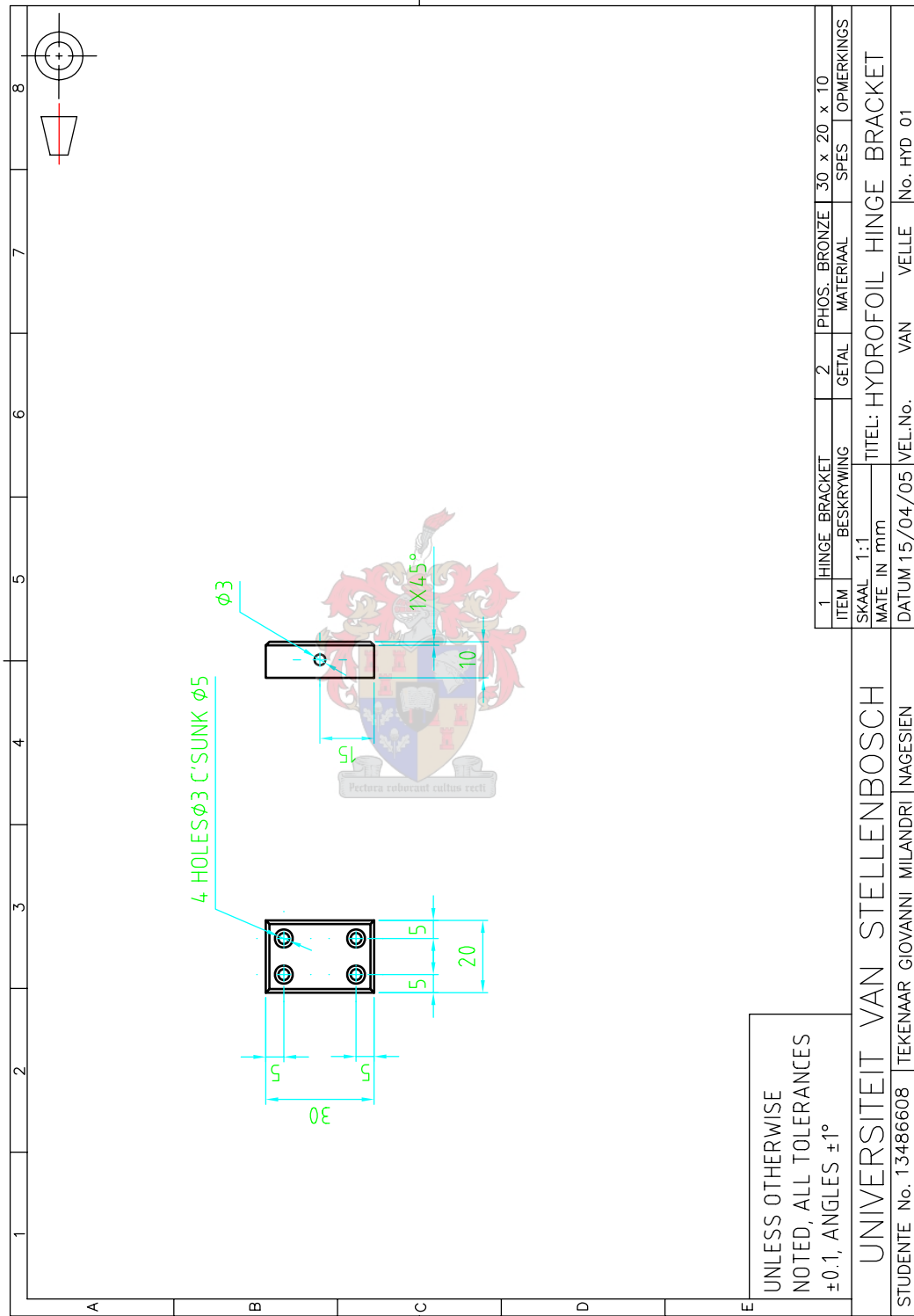


Figure C.4: Hydrofoil hinge bracket drawing

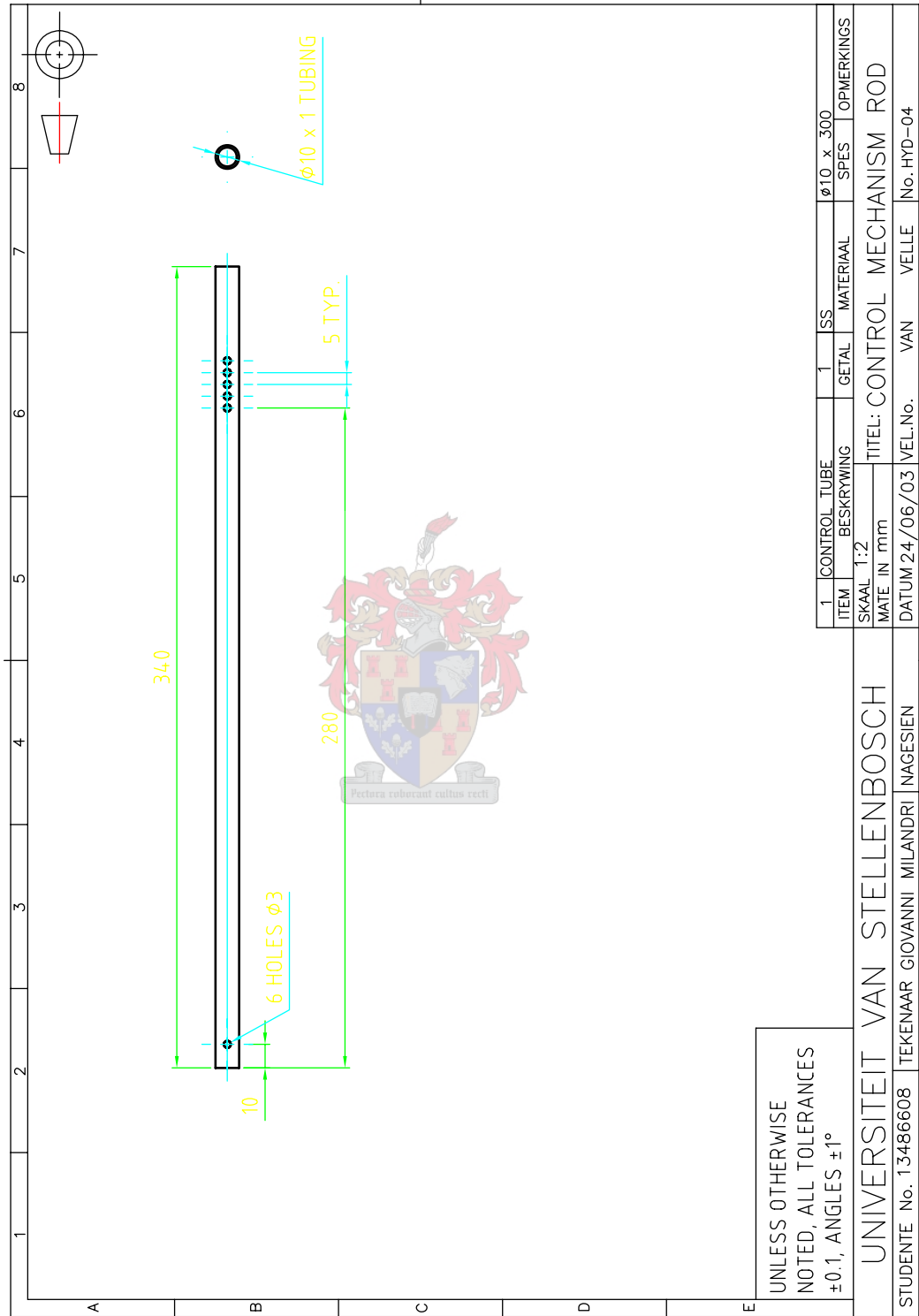


Figure C.5: Hydrofoil control rod drawing

Appendix D

Servo drive user instructions

